AMERICAN JOURNAL OF PHYSIOLOGY
LUNG CELLULAR AND MOLECULAR PHYSIOLOGY

Am J Physiol Lung Cell Mol Physiol 328: L413–L429, 2025.
First published February 4, 2025; doi:10.1152/ajplung.00274.2024

RESEARCH ARTICLE

Pulmonary vascular remodeling in Fra-2 transgenic mice is driven by type 2 inflammation and accompanied by pulmonary vascular hyperresponsiveness

Anna Birnhuber,[1,2] Valentina Biasin,[1,2,3] Pritesh P. Jain,[1] Grzegorz Kwiatkowski,[4] Ekaterina Boiarina,[5] Jochen Wilhelm,[6] Katharina Ahrens,[5] Chandran Nagaraj,[1] Andrea Olschewski,[1,7] Martin Witzenrath,[5,8] Stefan Chlopicki,[4,9] Leigh M. Marsh,[1,2] Christoph Tabeling,[5,10]* and Grazyna Kwapiszewska[1,2,6]*

[1]*Ludwig Boltzmann Institute for Lung Vascular Research Graz, Graz, Austria;* [2]*Otto Loewi Research Center, Lung Research Cluster, Medical University of Graz, Graz, Austria;* [3]*Division of Physiology and Pathophysiology, Otto Loewi Research Center, Medical University of Graz, Graz, Austria;* [4]*Jagiellonian Centre for Experimental Therapeutics, Jagiellonian University, Krakow, Poland;* [5]*Department of Infectious Diseases, Respiratory Medicine and Critical Care, Charité – Universitätsmedizin Berlin, Corporate Member of Freie Universität Berlin and Humboldt-Universität zu Berlin, Berlin, Germany;* [6]*Institute for Lung Health, Cardio-Pulmonary Institute, German Center for Lung Research, Justus-Liebig-University Giessen, Giessen, Germany;* [7]*Department of Anesthesiology and Intensive Care Medicine, Medical University of Graz, Graz, Austria;* [8]*German Center for Lung Research (DZL), Berlin, Germany;* [9]*Faculty of Medicine, Chair of Pharmacology, Jagiellonian University Medical College, Krakow, Poland; and* [10]*Berlin Institute of Health at Charité—Universitätsmedizin Berlin, Berlin, Germany*

Abstract

Lung vessel remodeling leads to increased pulmonary vascular resistance, causing pulmonary arterial hypertension (PAH), and consequently right ventricular hypertrophy and failure. In patients suffering from systemic sclerosis (SSc), PAH can occur and is a life-threatening complication. Dysregulation of immune processes plays a crucial role in pulmonary vascular remodeling, as has previously been shown in Fos-related antigen-2 (Fra-2) transgenic (TG) mice, a model of SSc-PAH. Here, we investigate whether vascular remodeling in the Fra-2 TG model is driven by type 2 inflammation and is associated with vascular hyperresponsiveness, an important feature of PAH pathobiology. Basal pulmonary arterial pressure and pulmonary vascular responsiveness to hypoxic ventilation and serotonin were increased in isolated, perfused, and ventilated lungs of Fra-2 TG mice compared with wild-type (WT) littermates. Similarly, contractile responses of isolated intrapulmonary arteries were elevated in Fra-2 TG mice. We also observed increased expression of contractile genes in Fra-2 overexpressing human pulmonary arterial smooth muscle cells (PASMCs) with elevated intracellular calcium levels after interleukin (IL)-13 stimulation. These findings were corroborated by transcriptomic data highlighting dysregulation of vascular smooth muscle cell contraction and type 2 inflammation in Fra-2 TG mice. In vivo, type 2-specific anti-inflammatory treatment with IL-13 neutralizing antibodies improved vascular remodeling in Fra-2 TG mice, similar to corticosteroid treatment with budesonide. Our results underscore the importance of type 2 inflammation and its potential therapeutic value in PAH-associated pulmonary vascular remodeling and hyperresponsiveness in SSc-PAH.

NEW & NOTEWORTHY In patients suffering from systemic sclerosis (SSc), pulmonary arterial hypertension (PAH) is a life-threatening complication linked to immune dysregulation. Preclinical analyses in Fos-related antigen-2 (Fra-2) transgenic (TG) mice, a model of SSc-PAH, identify type 2 inflammation as a key driver of vascular remodeling. Anti-inflammatory treatment targeting type 2 inflammation via IL-13 neutralizing antibodies improved pulmonary vascular remodeling. Thus, type 2-specific anti-inflammatory treatment may be a promising therapeutic approach in SSc-PAH.

hypoxic pulmonary vasoconstriction; pulmonary hypertension; type 2 inflammation; vascular hyperresponsiveness; vascular remodeling

INTRODUCTION

Pulmonary vascular remodeling is the pivotal structural alteration in pulmonary arterial hypertension (PAH) (1). PAH can be idiopathic (with unknown cause) or result from multiple causes, including autoimmune and infectious diseases (2–5). It is associated with increased pulmonary arterial pressure, ultimately leading to right ventricular hypertrophy, right heart failure, and eventually death (6–8).

In patients with systemic sclerosis (SSc), the presence of PAH significantly affects the clinical course and overall survival rate, since it is the single most common cause of death

*C. Tabeling and G. Kwapiszewska contributed equally to this work.
Correspondence: G. Kwapiszewska (Grazyna.Kwapiszewska-marsh@medunigraz.at).
Submitted 19 August 2024 / Revised 4 September 2024 / Accepted 17 January 2025

in these individuals (9). Despite remarkable advances in elucidating the pathogenesis of PAH over the past two decades, therapy venues are nonetheless still insufficient in SSc-related PAH (SSc-PAH), and the average survival time of patients with this condition usually does not exceed 4 years (10).

Multiple cell types play a role in the remodeling of the pulmonary vasculature, such as vascular endothelial cells, smooth muscle cells, and various immune cells (11, 12). There is strong evidence that dysregulation of immune processes plays a critical role in the development of pulmonary vascular remodeling and pulmonary hypertension (13, 14).

Mounting evidence indicates that type 2 immune signaling is upregulated in PAH (2, 15) as well as in pulmonary fibrosis (16). Furthermore, hallmarks of PAH were demonstrated and confirmed in various murine models of type 2-driven inflammation, including pulmonary vascular hyperresponsiveness, increase in right ventricular systolic pressure, pulmonary vascular remodeling, and right ventricular hypertrophy (5, 15, 17–22). Fra-2 transgenic (TG) mice (23) manifest systemic fibrotic disease characterized by enhanced pulmonary collagen deposition and restrictive lung disease (24, 25). In addition, Fra-2 TG mice display increased pulmonary vascular muscularization and pulmonary hypertension (25–27). These features mirror the characteristics observed in SSc-PAH (25, 28, 29). In Fra-2 TG mice, the respective vascular alterations occur at early time points before the development of pulmonary fibrosis. Fra-2 TG mice have been previously found to possess a pronounced type 2 signature with high levels of eosinophils and cytokines such as interleukin (IL)-13 and IL-4 in the lung tissue and bronchoalveolar compartments (25, 30, 31), as well as increased numbers of Th2-polarized $CD4^+$ T cells (32).

In this study, we investigated whether the early vascular remodeling processes in the Fra-2 TG mouse model are driven by type 2 inflammation and whether they are accompanied by increased vascular hyperresponsiveness, using a combination of in vivo, ex vivo, and in vitro experiments. We observed early, type 2-predominant eosinophilic inflammation in Fra-2 TG mice and an alteration of pulmonary arterial smooth muscle cell (PASMC) contractility by Fra-2 expression in the setting of type 2 inflammation. In addition, we found vascular remodeling to be ameliorated by anti-inflammatory treatment using type 2-specific anti-IL-13 blocking antibodies in the Fra-2 TG mouse model.

MATERIALS AND METHODS

Animal Experiments

Fra-2 transgenic (TG) mice (RRID:MGI:5656158) were obtained from Erwin Wagner, Research Institute of Molecular Pathology, Vienna, and bred in-house (23). Mice were maintained under specific pathogen-free conditions in isolated ventilated cages with 12-h light/dark cycles. Water and food were supplied ad libitum. All mouse experiments were ethically approved by local governmental and institutional authorities, and all measures were taken to keep animal suffering to a minimum. Experiments were conducted in female mice because inflammation and extracellular matrix expression are more pronounced and consistent in female Fra-2 overexpressing mice compared with their male littermates, reflecting the female predisposition observed in human SSc. The characterization of the TG phenotype was performed in 8- and 16-wk-old female mice in two independent experiments with 5–7 mice/group. Whenever feasible, investigators were blinded to the experimental groups. However, the pronounced phenotype of the Fra-2 TG mice posed limitations to the extent of blinding. To block IL-13 activity, 150 μg of rat anti-mouse IL-13 (IgG1κ) antibody (clone eBio1316H; Thermo Fisher Scientific, Waltham, MA) per mouse was injected intraperitoneally twice a week. Control mice received 150 μg of rat IgG1κ isotype control (clone RTK2071). To investigate the effect of glucocorticosteroid treatment, 10 μg of budesonide (Pulmicort suspension; AstraZeneca, Cambridge, UK) per mouse, or PBS as a control, was applied intranasally three times a week. Both treatments were initiated in 10–11-wk-old mice. Fra-2 TG mice were randomly assigned to treatment groups. Organ collection was performed after 6 wk of treatment. Anti-IL-13 and glucocorticosteroid treatments were performed once with 5–8 animals/group. A detailed description of the experimental setup was previously published (31).

Assessment of Blood Flow Velocity in the Pulmonary Artery

A Doppler flow velocity system (Indus Instruments, Houston, TX) with a 20 MHz single-transceiver Doppler probe was used, as described previously (33). Anesthesia was administered through a nose cone at a concentration of 1.0%–1.25% isoflurane in oxygen. The animals were positioned in a supine orientation on a heating pad and secured to a four-channel ECG system using a tape on each paw. An endorectal probe was placed for continuous monitoring of body temperature. The upper chest was shaved, and ultrasound gel was applied to both the chest and the Doppler probe. The probe was manually adjusted and secured using a micromanipulator. Its proper alignment along the pulmonary artery was verified by visually inspecting the blood flow velocity waveform in relation to the ECG signal. The probe was oriented perpendicularly to the sternum and tilted toward the animal's right side. Blood flow velocity was recorded for 2,000 ms, capturing 16–20 blood flow speckles. Speckles recorded during expiration were included in the analysis, and an average of 3–5 speckles/animal was used. Data analysis was performed using the vendor-provided software (Indus Instruments).

Magnetic Resonance Imaging of Right Ventricle

All magnetic resonance (MR) experiments were recorded with a 9.4 T small animal magnetic resonance imaging (MRI) scanner (Bruker BioSpec, Ettlingen, Germany) equipped with a 36-mm quadrature volume coil. During the experiment, mice were anesthetized using isoflurane (1.5–2 vol%) in an oxygen and air (1:2) mixture. Body temperature was monitored with an endorectal probe and maintained in the range of 35.5°C–36.5°C. To evaluate the global right ventricular (RV) function, the bright-blood cine images were collated in 6–8 contiguous slices covering the whole ventricle volume using a flow-compensated, prospectively gated gradient-echo FLASH sequence (FOV 30×30 mm^2, acquisition matrix 128×128, TE/TR = 2.3/5 ms, 1 mm slice thickness, number of

averages = 8, flip angle = 11°). Depending on the heart rate, between 22 and 24 cine frames were acquired. All data were analyzed offline using ImageJ (34). Endo- and epicardial contours were manually segmented and used to calculate RV mass (assuming a tissue density of 1.05 g/cm^3); end-systolic volume (ESV) and end-diastolic volume (EDV) were used to calculate stroke volume, SV = EDV − ESV and ejection fraction, EF = 100 × (EDV − ESV)/EDV.

Histology Staining and Quantification

Formalin-fixed and paraffin-embedded mouse lungs were cut into 2.5 μm sections for histological analysis. Sections were deparaffinized in xylene followed by decreasing concentrations of ethanol. Sirius red staining was performed according to the standard protocols. In short, slides were incubated first in 0.2% phosphomolybdic acid for 4 min, then in picrosirius red solution (Gatt Koller, Absam, Austria) for 30 min, followed by differentiation in 0.5% acetic acid. Antigen retrieval for immunostainings was performed using citrate buffer (pH 6) at 95°C for 20 min. Primary antibodies against phospho-STAT6 (1:100, Cat. No. 9361; Cell Signaling Technology, RRID:AB_331595), smooth muscle actin (SMA; 1:30,000, Cat. No. A2547; Sigma-Aldrich, RRID:AB_476701), or von Willebrand factor (vWF; 1:10,000, Cat. No. A0082; Agilent, RRID:AB_2315602) were incubated for 1 h at room temperature. Primary antibodies were detected by the immPRESS α-rabbit Ig (peroxidase) polymer detection kit using DAB peroxidase (HRP) substrate. SMA was detected using the Vector Vip Peroxidase (HRP) substrate kit (Vector Laboratories, Burlingame, CA). Counterstaining was performed for 10 s in 0.05% methyl green in 0.1 M sodium acetate trihydrate (Sigma Aldrich, St. Louis, MO). Images were obtained using an Olympus VS120 slide scanning microscope at ×40 magnification.

Tissue sections were analyzed using Visiopharm integrated software VIS (Visiopharm, Denmark). The degree of muscularization and vessel wall thickness were analyzed on tissue sections double-stained with vWF and SMA, as described previously (24, 25, 27). In short, the length of SMA staining relative to the vessel circumference was used to calculate the degree of muscularization. Vessel wall thickness was calculated by dividing the area of vWF and SMA staining by the vessel circumference. In total, 211 ± 84 (minimum: 39, maximum 431) vessels were analyzed per mouse. Of note, relative proportions of non-, partially, or fully muscularized vessels can vary between different staining batches; therefore, all samples shown in one graph were stained and analyzed at the same time.

Immunofluorescence Staining

Sections (2.5 μm) of Formalin-fixed and paraffin-embedded mouse lungs were deparaffinized and rehydrated in decreasing concentrations of ethanol. Antigen retrieval was performed using citrate buffer (pH 6) followed by two separate blocking steps using BLOXALL (Vector Laboratories) and 2.5% horse serum. Slides were sequentially incubated overnight with primary antibodies directed against CD45 (1:250, Cat. No. ab10558; Abcam, RRID:AB_442810) and Collagen I (1:500, Cat. No. 1310-01; SouthernBiotech, RRID:AB_2753206), or Arg1 (1:205, Cat. No. sc-271430; Santa Cruz Biotechnology, RRID:AB_10648473) and developed using the Opal detection system (Akoya Biosciences, Marlborough, MA). vWF primary antibody (1:100, Cat. No. A0082; Agilent, RRID:AB_2315602) was incubated overnight followed by the secondary antibody labeled with AF555 and SMA-FITC labeled primary antibody (1:300, Cat. No. F3777; Sigma-Aldrich, RRID:AB_476977). Finally, slides were stained with DAPI for visualization of nuclei and mounted with DAKO fluorescence mounting medium. In parallel, negative controls were performed by omission of the first antibody. Image acquisition was performed on a SP8 fluorescence confocal microscope (Leica). For images within one figure, slides were stained simultaneously and images were acquired at the same time using the same exposure times and settings.

Bronchoalveolar Lavage and Flow Cytometry

Bronchoalveolar lavage (BAL) was performed using 1 mL PBS with protease inhibitor cocktail (Roche) and 1 mM EDTA. BAL fluid (BALF) was centrifuged to pellet BALF cells, and total and viable cell counts were obtained. Cells were stained using a viability dye and antibodies directed against CD45, CD19, CD3, Siglec-F, and CD11c. Antibody details are provided in Table 1. Data were acquired using a Cytoflex S (Beckman Coulter, CA). Viable cells were initially gated on CD45 positivity and were identified as follows: T cells (CD3$^+$), B cells (CD19$^+$), alveolar macrophages (CD11c$^+$, Siglec-F$^+$), and eosinophils (CD11c$^-$, Siglec-F$^+$).

Transcriptomic Analysis

Total RNA was isolated from lungs of female 8-wk-old Fra-2 TG and wild-type (WT) littermate control mice (4 animals/group) using the RNeasy Mini kit (Peqlab, Erlangen, Germany). Total RNA (200 ng) was preamplified and labeled with Cy5 using the low-input QuickAmp kit (Agilent Technology, Santa Clara, CA) according to the manufacturer's instructions. Hybridizations were performed for 18 h at 42°C on Agilent 6x80K mouse microarrays in Agilent hybridization chambers. Data were analyzed using the limma package in R (35). Intensity values were background-corrected and quantile normalized. The significance of differential expression was estimated using moderated *t*-statistics as previously described in detail (36). Data visualization was performed in R programming environment (37). Heat maps were computed using "pheatmap" package version 1.0.12 (38).

Isolated Perfused and Ventilated Mouse Lung

Fourteen- to seventeen-week-old female mice were used for isolated perfused and ventilated mouse lung (IPL) experiments. Lungs were isolated, and cannulation of the pulmonary artery and left atrium was performed. Nonrecirculating perfusion (1 mL/min, 37°C) with sterile Krebs–Henseleit

Table 1. *List of antibodies used for flow cytometry*

Target	Fluorophore	Clone	Source	RRid
CD45	AF700	30-F11	BD Biosciences	AB_1645208
CD19	APC-Cy7	6D5	BioLegend	AB_2922473
Siglec-F	PE	E50-2440	BD Biosciences	AB_394341
CD11c	ef450	N418	Thermo Fisher	AB_1548654
CD3e	BV510	145-2C11	BioLegend	AB_2565879

hydroxyethyl amylopectin buffer (Serag-Wiesner, Naila, Germany) and volume-controlled (tidal volume of ~10 mL/kg body wt) negative pressure ventilation (end-expiratory pressure −2 cmH_2O, 90 breaths/min) were established. Hyperinflation (−24 cmH_2O) intervals were set to 4 min (39). Pulmonary arterial pressure (Ppa) was constantly recorded.

For analysis of hypoxic pulmonary vasoconstriction (HPV), N^{ω}-nitro-L-arginine methyl ester hydrochloride (1 mM) and indomethacin (30 μM, both Sigma-Aldrich, Steinheim, Germany) were added to the buffer (40). A four-point pressure-flow (P-Q) curve was performed under normoxic baseline conditions by altering the perfusion flow every 30 s from 0.5 to 1.0 to 1.5 to 2.0 mL/min (41). The perfusion rate was reset to 1 mL/min. Hypoxic ventilation (1% O_2) was initiated to assess HPV, and 10 min later a second P-Q curve was performed (42). For serotonin-induced vasoconstriction, serotonin was added to the perfusion buffer at concentrations of 10 nM, 100 nM, 1 μM, or 10 μM and lungs were perfused with each concentration for 1 min followed by a 10 min wash-out period with perfusion buffer.

The maximal increase in Ppa due to the respective vasoconstrictive stimulus was computed (Δ Ppa). Data were excluded from further analyses if lungs had signs of hemostasis, atelectasis, edema, or if maximal HPV response was <2 cmH_2O.

Wire Myography

Ten to twelve wk old, female Fra-2 TG and WT littermates were used for wire myograph. The tertiary intrapulmonary arteries (PAs) were isolated via stereo zoom microscope SZX7 (Olympus Corp, Tokyo, Japan) as described (43, 44). PAs were mounted on the jaws in myograph chambers (Multi Wire Myograph System-620M; Danish MyoTechnology A/S, Aarhus, Denmark), equilibrated, and tested for viability, and dose-response curve analyses with potassium chloride (KCl) and thromboxane analogue U-46619 were performed as reported (44, 45). Measurements were analyzed with PowerLab 8/35 (AD Instruments, Dunedin, New Zealand).

Cell Culture of Pulmonary Arterial Smooth Muscle Cells

Primary human pulmonary arterial smooth muscle cells (PASMCs) were isolated from pulmonary arteries from non-transplanted donor lungs. The protocol and tissue usage were approved by the local authorities [Vienna Institutional Ethics Committee (976/2010 and EK 1417/2022]. Comprehensive details regarding donor characteristics are provided in Supplemental Table S1. The purity of PASMC cultures was confirmed using immunofluorescent antibody staining for smooth muscle-specific isoforms of α-actin (minimum 95% of cells stained positive). PASMCs were grown in full medium (VascuLife SMC Complete Kit; LifeLine Technology). All experiments were performed in cells in passages 2–6, and cells were growth-arrested by serum deprivation for 12 h.

Transfection

PASMCs were transfected with overexpression vectors pCDNA3.1 containing the human *Fosl2/Fra-2* gene under the control of a cytomegalovirus promotor. The empty vector served as vehicle control (Ctrl). Transfection was achieved using JetPrime transfection reagent according to the manufacturer's instructions. In short, PASMCs were incubated with the transfection mix in full medium for 4 h, followed by a medium change and further experiments.

Proliferation Measurements

Following transfection with Ctrl or Fra-2 overexpression plasmids, PASMCs were seeded in 96-well plates (5,000–10,000 cells/well) and grown overnight to enable proper attachment. Following 12 h of starvation in basal medium, cells were treated with IL-13 (50 ng/mL) and 5-ethynyl-2′-deoxyuridine (EdU, 10 μM) to label proliferating cells. Basal and full medium (supplemented with EdU) served as negative and positive controls, respectively. After 24 h, cells were washed twice with PBS and fixed with 4% paraformaldehyde (PFA) for 15 min at room temperature. Following fixation, cells were washed twice with PBS, permeabilized with 0.1% Triton-X in PBS for 20 min at room temperature, and stained with the baseclick EdU Cell Proliferation kit 488 (baseclick GmbH) according to the manufacturer's instructions. Nuclei were stained with Hoechst reagent (1:1,000) for 30 min. Cells were imaged using the ImageXpress Pico Automated Cell Imaging System (Molecular Devices) at ×10 magnification and analyzed with the CellReporterXpress Software Version 2.7 (Molecular Devices).

Intracellular Calcium Measurement

Ctrl and Fra-2 plasmid transfected cells were seeded on 96-well plates and loaded with Fluo4 for 40 min at 37°C. EGTA (120 mM) was used to evaluate background signal, and ionomycin (5 μM) was used to assess the total calcium release. Data were acquired on a CLARIOstar plate reader (BMG Labtech) using an excitation/emission wavelength of 490 and 510 nm, respectively.

RNA Isolation and Real-Time RT-PCR

Total RNA was isolated from lung homogenates using the peqGOLD Total RNA kit (Peqlab, Germany). Reverse transcription was performed using the iScript cDNA synthesis kit (Bio-Rad). The real-time RT-PCR reaction was run on a LightCycler 480 System (Roche Applied Science, Austria) using the QuantiFast SYBR Green PCR kit (Qiagen, Germany). Hydroxymethylbilane synthase (*Hmbs*) and beta-2-microglobulin (*B2m*) were used as reference genes. Differences of threshold cycle (Ct) were calculated as follows: ΔCt = mean Ct reference genes − Ct target gene. Primer sequences are given in Table 2.

Western Blot

Protein lysates Ctrl or Fra-2 plasmid transfected PASMCs were isolated using RIPA buffer (Sigma). Protein samples were separated by SDS-PAGE and transferred to PVDF membranes (GE Healthcare, UK). Membranes were incubated with primary antibodies [Fosl2 (HPA004817), 1:1,000; Atlas Antibodies/pMLC, MLC, RhoA, and α-tubulin, 1:1,000; Cell Signaling Technologies] at 4°C overnight, followed by 1 h incubation at room temperature with HRP-conjugated secondary antibodies. Membranes were incubated with ECL prime developing solution (GE Healthcare, UK). Signal detection was performed using a ChemiDoc Touch Imaging System (Bio-Rad). Uncropped images of membranes are shown in Supplemental Fig S1.

Table 2. *Primer sequences used for RT-PCR*

Gene	Gene Symbol	Species	Primer Sequence 5′-3′	Primer Sequence 5′-3′
Arginase 1	*Arg1*	mouse	TTTCTCAAAAGGACAGCCTCG	CACAGACCGTGGGTTCTTCA
Arginase 2	*Arg2*	mouse	CCACTCCTAGCTTCTTCTGTCC	TCCTCCACGGGCAAATTCC
Nitric oxide synthase 3	*Nos3*	mouse	CTCCAGCACCGGAGCCTA	TACAGGGCCCATCCTGCT
Beta-2-microglobulin	*B2m*	mouse	CGGCCTGTATGCTATCCAGAAAACC	TGTGAGGCGGGTGGAACTGTG
Hydroxymethylbilane synthase	*Hmbs*	mouse	TCCGGAGGCGGGTGTTGAGG	GCCAGAGAAAAGTGCCGTGGG
Ras homolog family member A	*RHOA*	human	AGCAAGCATGTCTTTCCACA	GAAGAGGCTGGACTCGGATT
Ras homolog family member B	*RHOB*	human	GGGACAGAAGTGCTTCACCT	CGACGTCATTCTCATGTGCT
Rho associated coiled-coil containing protein kinase 1	*ROCK1*	human	GGCAGGAAAATCCAAATCAT	AAAAATGGACAACCTGCTGC
Rho associated coiled-coil containing protein kinase 2	*ROCK2*	human	TTGTTTTTCCTCAAAGCAGGA	CGCTGATCCGAGACCCT
Arginase 1	*ARG1*	human	TCAAAGGGACAGCCACGAG	TAGGGATGTCAGCAAAGGGC
Beta-2-microglobulin	*B2M*	human	CCTGGAGGCTATCCAGCGTACTCC	TGTCGGATGGATGAAACCCAGACA
Hydroxymethylbilane synthase	*HMBS*	human	CTGCAACGGCGGAAGAAAA	AATCTTGTCCCCTGTGGTGG

NO Measurements

Lung tissue was freshly processed by homogenization in PBS at a 1:10 ratio using a Dounce homogenizer, followed by centrifugation at 10,000 rpm for 10 min at 4°C as recommended by the manufacturer. Nitrite (NO_2^-) levels reflecting nitric oxide (NO) bioavailability in the lung tissue were measured immediately after homogenization using the NO colorimetric assay kit (Elabscience, Cat. No. E-BC-K035-M) according to the manufacturer's protocol.

Statistical Analysis

Statistical analysis was performed in GraphPad Prism 6 software (Graph Pad Software Inc.). Data are expressed as single data points with box plot overlay (whiskers indicating minimum/maximum values), if not stated otherwise. Muscularization data are shown as bar graphs (means + SD). Comparisons between two groups with equal variances were performed using an unpaired Student's *t* test. Groups with different variances were compared using Welsh's *t* test. Treatment effects of WT and Fra-2 TG samples were analyzed by two-way ANOVA and post-tests for multiple comparisons. Statistical tests for specific data sets are provided in the figure legends. *P* values below 0.05 were considered as statistically significant.

RESULTS

Enhanced Muscularization, Perivascular Collagen Deposition, and Altered Pulmonary Artery Blood Flow in Fra-2 TG Mice

Fra-2 transgenic (TG) mice were analyzed at two different time points. The first analysis was performed in young mice before the development of pulmonary fibrosis (8 wk of age), and the second when fibrotic changes in the lungs were starting to become manifest (16 wk of age) (Fig. 1*A*). Collagen staining using picrosirius red revealed increased perivascular collagen deposition in 8-wk-old Fra-2 TG mice which was further exacerbated in 16-wk-old Fra-2 TG mice compared with littermate wild-type (WT) control mice (Fig. 1*B*, *upper*). Quantification of muscularization as indicated by the ratio of the length of α-SMA (marking smooth muscle cells) per length of total vessel wall, (Fig. 1*B*, *lower*) showed an increased proportion of partially and fully muscularized vessels with a concomitant decrease of nonmuscularized vessels in both time points (Fig. 1*C*). Despite increased muscularization of vessels, the vessel wall thickness was not altered in Fra-2 TG mice at 8 wk but increased by trend in 16-wk-old mice (Fig. 1*D*).

We further conducted in vivo Doppler blood flow velocity mapping in the pulmonary artery of Fra-2 TG and WT mice. Similar to patients with PAH, the pattern of the pulsed-wave Doppler of the pulmonary artery blood flow appeared triangular in 16-wk-old Fra-2 TG mice, in contrast to the more dome-like pattern in WT mice (Fig. 1*E*) (46–49). Elevated pulmonary arterial pressure (Ppa) results in premature closing of the pulmonary valve. Therefore, pulmonary acceleration time (PAT) is shortened. Importantly, PAT inversely correlates with pulmonary arterial pressure (47, 50). In line, a decrease in PAT could be observed in Fra-2 TG mice before fibrosis development at 8 wk of age compared with WT control mice, with further deterioration observed by 16 wk of age (Fig. 1*F*). These changes underscore the functional significance of the PH-associated pulmonary vascular pathologies observed in Fra-2 TG mice.

Fra-2 TG Mice Show Right Ventricular Dysfunction in MRI

To further assess the functional significance of vascular remodeling in this mouse model, we conducted in vivo cardiac magnetic resonance imaging (MRI) to evaluate right ventricular function. In concordance with the previously reported increase of the RV/(LV + S) ratio (Fulton index) of Fra-2 TG mice (26), MRI of the right ventricle (Fig. 2, *A* and *B*) revealed an increased RV mass in Fra-2 TG mice (Fig. 2*C*). End-diastolic right ventricular volume was not significantly altered, with a trend toward increased volumes in Fra-2 TG mice (Fig. 2*D*). However, the end-systolic volume of the right ventricle was significantly elevated in Fra-2 TG mice already at the age of 8 wk and was even more pronounced at 16 wk of age (Fig. 2*E*). RV stroke volume was similar between Fra-2 TG and WT mice (Fig. 2*F*), but the RV ejection fraction was reduced in Fra-2 TG mice at 16 wk of age (Fig. 2*G*).

Lungs of Fra-2 TG Mice Exhibit Stimulus-Independent Vascular Hyperresponsiveness

To clarify the cause of functional impairment in Fra-2 TG mice, we investigated whether it resulted from increased stiffness and decreased vascular compliance linked to the

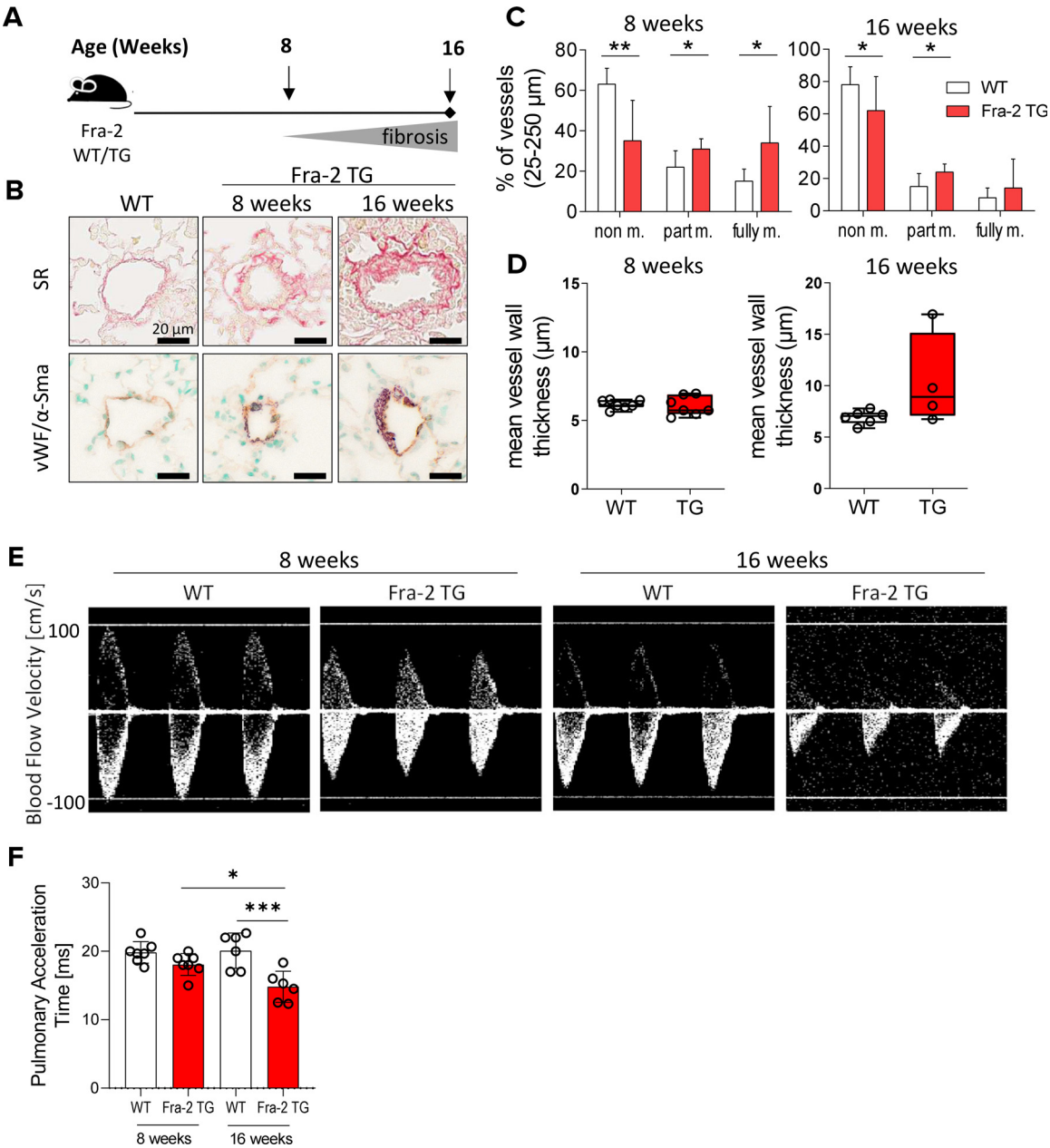

Figure 1. Fra-2 overexpression in mice leads to increased pulmonary vascular remodeling and altered pulmonary artery blood flow velocity. *A*: schematic representation of experimental setup using Fra-2 transgenic (TG) and wild-type (WT) littermate control mice. *B*: collagen (picrosirius red) and von Willebrand factor (vWF)/α-smooth muscle actin (α-SMA) double staining of pulmonary vessels in Fra-2 TG or WT control mice at the age of 8 or 16 wk. *C*: quantification of muscularization of small pulmonary vessels (25–250 µm diameter) in 8- and 16-wk-old WT ($n = 7$) and Fra-2 TG ($n = 7/4$) mice. Non-m., non-muscularized, part m., partially muscularized, fully m., fully muscularized. Unpaired *t* tests were used to analyze the difference of non, partially, and fully muscularized vessels in WT and Fra-2 TG mice. $^*P < 0.05$, $^{**}P < 0.01$. *D*: quantification of mean vessel wall thickness in 8 (*left*) and 16 (*right*) wk old Fra-2 TG and WT mice. Each datapoint represents one animal ($n = 4–6$). *E*: representative images of Doppler blood flow velocity waveforms in Fra-2 TG and WT control mice at 8 and 16 wk of age. *F*: pulmonary acceleration time of pulmonary arteries in Fra-2 TG and WT mice. Each datapoint represents one animal ($n = 6–8$). One way-ANOVA with Sidak's multiple comparison test, $^*P < 0.05$, $^{***}P < 0.001$. Fra-2, Fos-related antigen-2.

observed remodeling, or from heightened pulmonary vascular responsiveness. We first examined whether the vascular changes observed in the histology of young Fra-2 TG mice were supported by gene expression alterations using transcriptome analysis. Targeted analysis of the gene ontology GO:0014829 (associated vascular smooth muscle contraction) revealed expression profile changes robust enough to distinguish the distinct groups: Unbiased hierarchical clustering of lung homogenates from 8-wk-old Fra-2 TG and WT mice clearly separated the two different genotypes (Fig. 3*A*), suggesting alterations in both the vascular morphology and the contractile properties. To assess the functional relevance of these findings, we performed ex vivo measurements of pulmonary vascular responsiveness in isolated, perfused, and ventilated mouse lungs (Fig. 3*B*) and in isolated intrapulmonary arteries using wire myography.

AJP-Lung Cell Mol Physiol • doi:10.1152/ajplung.00274.2024 • www.ajplung.org

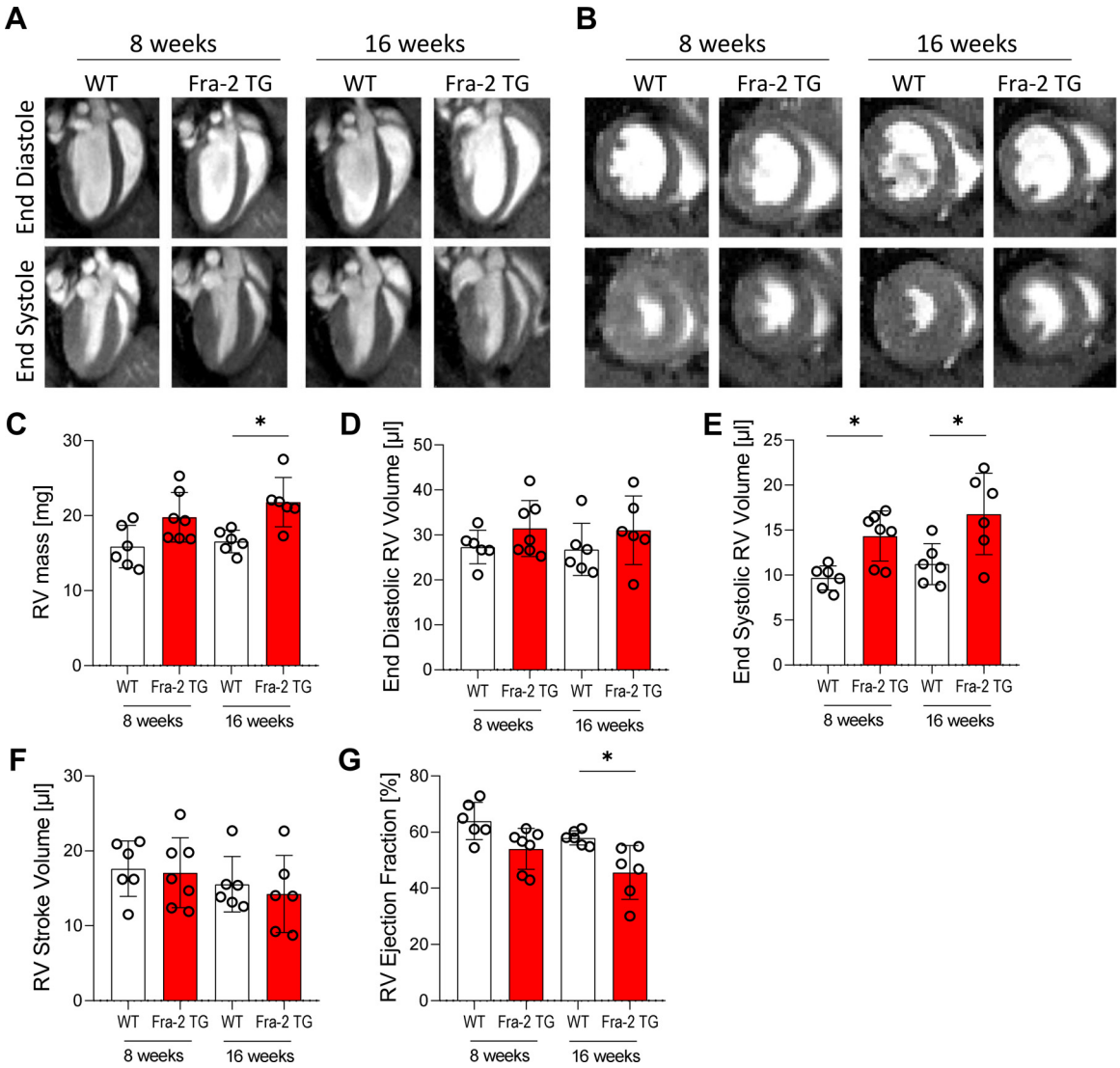

Figure 2. Fra-2 transgenic mice possess altered right ventricular function. *A* and *B*: representative images of cardiac MRI of Fra-2 transgenic (TG) and wildtype (WT) litter mate control mice at 8 and 16 wk of age. *C–G*: analysis of right ventricular (RV) mass (*C*), end-diastolic RV volume (*D*), end-systolic RV volume (*E*), RV stroke volume (*F*), and RV ejection fraction (*G*) of 8- and 16-wk-old Fra-2 TG and WT control mice. Each datapoint represents one animal ($n = 6–7$). One-way ANOVA with Sidak's multiple comparison test, $^*P < 0.05$. Fra-2, Fos-related antigen-2; MRI, magnetic resonance imaging.

In line with our previous studies (26), pulmonary arterial pressure (Ppa) at baseline was increased in isolated perfused lungs of Fra-2 TG mice compared with WT mice (Fig. 3*C*). In addition, hypoxic pulmonary vasoconstriction (HPV) was highly elevated in Fra-2 TG mice (Fig. 3*D*), with a significantly higher maximum increase of Ppa mean following ventilation with 1% oxygen in Fra-2 TG compared with WT lungs (Fig. 3*E*). Perfusion of the vascular system with serotonin (5-hydroxytryptamin, 5-HT) increased the Ppa mean in a dose-dependent manner in both WT and Fra-2 TG mice, but to a higher degree in Fra-2 TG mice (Fig. 3*F*).

Using a wire myograph (Fig. 3*G*), the contractile responses of intrapulmonary arteries isolated from Fra-2 TG or WT mice were further assessed in response to increasing doses of potassium chloride (KCl) or thromboxane analogue U-46619. Increasing doses of KCl or U-46619 led to a significant increase in contraction of pulmonary arteries isolated from Fra-2 TG mice compared with those isolated from WT mice (Fig. 3, *H* and *L*).

These data indicate pulmonary vascular hyperresponsiveness in Fra-2 TG mice irrespective of the vasoconstrictive stimulus.

Early Type 2 Predominant Eosinophilic Inflammation in Fra-2 TG Mice

Tissue remodeling and airway hyperresponsiveness have been previously linked to IL-13 (51). Moreover, we were previously able to show that at 16 wk of age, Fra-2 TG mice exhibit severe type 2 inflammation with high levels of IL-13 (31). Here, we therefore investigated inflammatory changes in young (8 wk) and adult (16 wk) Fra-2 TG mice. Multicolor immunofluorescence imaging confirmed increased collagen deposition and muscularization in the pulmonary vasculature of Fra-2 TG mice, in addition to revealing severe

perivascular inflammatory infiltrates in 16-wk-old Fra-2 TG mice (Fig. 4*A*). At 8 wk of age, there were no changes in BALF inflammatory cell counts between Fra-2 TG and WT mice; however, at 16 wk of age, a significant increase in inflammatory cell infiltration into the alveolar space was observed (Fig. 4*B*). Despite the lack of changes in total BALF cell counts at 8 wk of age, flow cytometric analysis revealed a shift of inflammatory cell populations. Although alveolar macrophage readings were lower, relative numbers of BALF eosinophils were increased in Fra-2 TG mice (Fig. 4*C*). This alteration was even more pronounced in 16-wk-old animals (Fig. 4*D*). Importantly, targeted expression analysis of genes

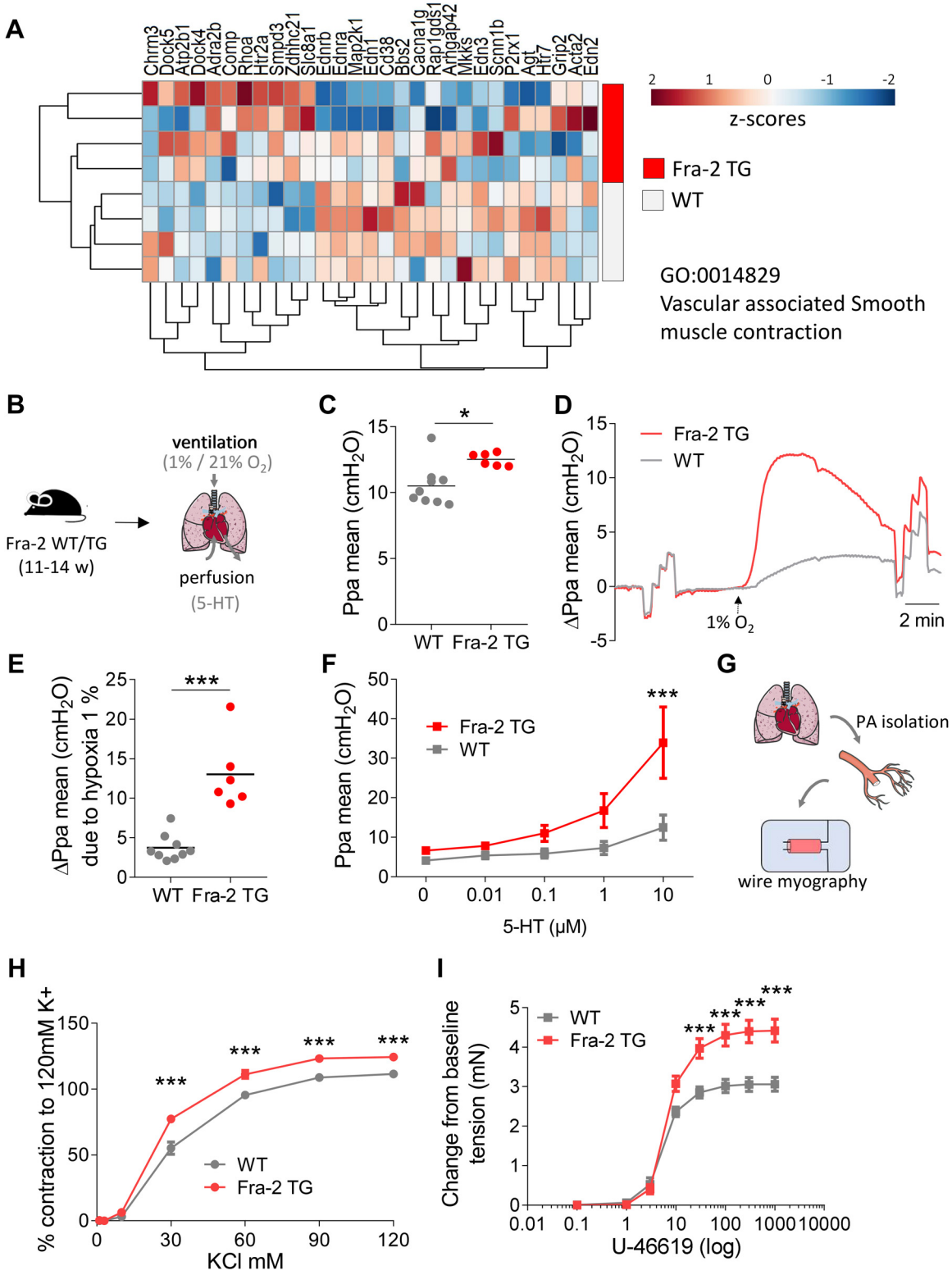

AJP-Lung Cell Mol Physiol • doi:10.1152/ajplung.00274.2024 • www.ajplung.org

associated with gene ontology GO:0042092 "type 2 immune response" in lung homogenates of 8-wk-old mice confirmed an early shift toward type 2 inflammation (Fig. 4*E*).

Pulmonary Arterial Smooth Muscle Cell Contractility Is Altered by Fra-2 Expression (in the Setting of Type 2 Inflammation)

To determine whether IL-13 signaling was operational in the vascular compartment of Fra-2 TG mice, we tested for phosphorylation/activation of Signal Transducer and Activator of Transcription 6 (Stat6) in respective samples. Immunohistochemical staining using antibodies directed against pStat6 revealed increased staining and nuclear localization in the vessel wall of remodeled vessels in Fra-2 TG mice (Fig. 5*A*, arrows). In contrast, almost no staining positivity could be observed in healthy WT lungs (Fig. 5*A*).

To assess the combined effects of Fra-2 and IL-13 on PASMC contraction, Fra-2 was overexpressed in human PASMCs in vitro, achieving a robust increase of Fra-2 up to 72 h (Fig. 5*B*). Of note, Fra-2 overexpression did not alter the proliferative phenotype of PASMCs at basal or stimulated conditions (Fig. 5*C*). We then analyzed genes from the contractile apparatus and observed a slight but significant increase of *RHOA, RHOB, ROCK1,* and *ROCK2* expression in PASMCs following Fra-2 overexpression, but no additive effect post IL-13 treatment (Fig. 5, *D–F*). In addition, intracellular Ca^{++} levels of normal or Fra-2 overexpressing PASMCs with or without IL-13 stimulation showed a significant synergistic effect leading to increased intracellular Ca^{++} in Fra-2 overexpressing PASMCs following IL-13 stimulation, as compared with control cells (Fig. 5*G*).

IL-13 has been previously reported to potentially influence contractile properties of PAs by causing an imbalance in arginine metabolism (52, 53). Targeted analysis of genes associated with the gene ontology GO:0006525 (arginine metabolic process) from transcriptome profiling of lung homogenates from 8-wk-old mice showed a clear clustering of WT samples compared with Fra-2 TG samples (Fig. 6*A*), indicating an imbalance in arginine metabolism already at a young age. We therefore analyzed expression levels of endothelial nitric oxide synthase (*Nos3/eNOS*), arginase 1 (*Arg1*), and *Arg2* in isolated pulmonary arteries (PAs) and in lung homogenates of 8- and 16-wk-old Fra-2 TG and WT control mice. In the lung homogenates of Fra-2 and WT mice, we observed a strong increase in *Arg1* expression, whereas *Nos3* levels were unaltered (Fig. 6*B*). *Arg2* expression was found to be unchanged at 8 wk of age, but decreased in Fra-2 TG mice at 16 wk of age compared with their littermate control mice (Fig. 6*B*). Similar changes were observed in PAs, where we found expression levels of *Nos3* and *Arg2* to be unaltered, whereas *Arg1* levels were significantly upregulated (Fig. 6*C*). To analyze whether these changes were due to alterations of gene expression levels in the smooth muscle layer of pulmonary arteries, we measured *ARG1* expression levels in cultured human PASMCs with or without Fra-2 overexpression. We did not observe any changes in *ARG1* expression levels (Fig. 6*D*). Immunofluorescence staining of arginase 1 and α-Sma showed no signal overlap but displayed distinct α-SMA-negative/Arg1-positive cells in close proximity and within the vessel wall in Fra-2 TG mice, indicating infiltrating inflammatory cells (Fig. 6*E*, white arrows), whereas almost no Arg1-positive cells were detected around PAs in healthy WT animals (Fig. 6*E*). In line with these observations, NO levels in the lung tissue of 16-wk-old Fra-2 mice appeared to be decreased. Although low levels of NO could be measured in the lungs of WT mice, they were below detection limit in 16-wk-old Fra-2 TG mouse lungs (Fig. 6*F*).

Our data show that pulmonary vascular hyperresponsiveness in Fra-2 TG mice results from two factors: increased pulmonary artery contractility due to Fra-2 activation in PASMCs, and an imbalance in arginine metabolism caused by elevated Arg1 levels in infiltrating immune cells, which reduces NO availability and enhances PA contraction in the lungs of Fra-2 TG mice.

Anti-Inflammatory Treatment Using Glucocorticosteroids or Type 2-Specific IL-13 Blocking Antibodies (Partially) Ameliorates Vascular Remodeling in the Fra-2 TG Mouse Model of SSc-PAH

To assess the type 2 dependence of the pulmonary vascular phenotype in vivo, we analyzed historical samples with unspecific suppression of inflammation using the glucocorticosteroid budesonide (Fig. 7*A*) or the pharmacological blockade of IL-13 signaling by IL-13 neutralizing antibodies (Fig. 7*E*) in Fra-2 TG mice. We have previously shown that both treatments decrease IL-13 signaling and phosphorylation of STAT6 in lung homogenates of Fra-2 TG mice (31). Here, budesonide treatment ameliorated the increased perivascular collagen deposition (Fig. 7*B*) and muscularization of pulmonary vessels in Fra-2 TG mice (Fig. 7, *B* and *C*). Mean vessel wall thickness was decreased by trend following administration of budesonide (Fig. 7*C*). In addition, expression levels of *Arg1* and *Arg2* were found to be decreased in lung homogenates of Fra-2 TG mice treated with budesonide, compared with Fra-2 TG mice without treatment (Fig. 7*D*). Similarly, administration of an anti-IL-13 blocking antibody was found to reduce perivascular collagen deposition (Fig. 7*F*) and to mitigate vascular remodeling (Fig. 7, *F* and *G*). No significant effects on expression levels of *Nos3*, *Arg1,* or *Arg2* were observed (Fig. 7*H*).

Figure 3. Pulmonary arteries of Fra-2 transgenic mice exhibit stimulus-independent vascular hyperresponsiveness. *A*: transcriptome analysis of lung homogenates of 8-wk-old Fra-2 transgenic (TG) or wild-type (WT) mice ($n = 4$): heatmap with unbiased hierarchical clustering of genes annotated to the gene ontology "vascular associated smooth muscle contraction" (GO:0014829), *z*-scores are shown. *B*: schematic representation of isolated perfused and ventilated mouse lung setup. IPL was conducted in mice 14 to 17 wk of age. *C*: mean pulmonary arterial pressure (Ppa mean) of isolated perfused mouse lungs of wildtype (WT; $n = 9$) or Fra-2 transgenic (Fra-2 TG; $n = 6$) mice at baseline. Unpaired *t* test, $^{*}P = 0.0101$. *D*: representative recording of flow-induced pressure changes in WT or Fra-2 TG mouse lungs under normoxic and hypoxic conditions (Ppa normalized to baseline). *E*: the maximum hypoxia-induced change of Ppa mean in WT ($n = 9$) and Fra-2 TG ($n = 6$) mouse lungs. Unpaired *t* test, $^{***}P < 0.001$. *F*: changes of Ppa mean in response to serotonin (5-hydroxytryptamin, 5-HT) administration to the perfusion buffer in isolated perfused lungs of WT ($n = 6$) or Fra-2 TG ($n = 7$) mice. *G*: schematic representation of pulmonary artery wire myography. *H* and *I*: assessment of vasoreactivity of the pulmonary arteries isolated from WT ($n = 3$) and Fra-2 TG ($n = 3$) mice upon dose-dependent stimulation with potassium chloride (KCl) (*H*) and thromboxane analog U-46619 (*I*). From each mouse, 3–4 PA segments were measured. *F–I*: two-way ANOVA with Bonferroni's multiple comparisons test, $^{***}P < 0.001$. Fra-2, Fos-related antigen-2.

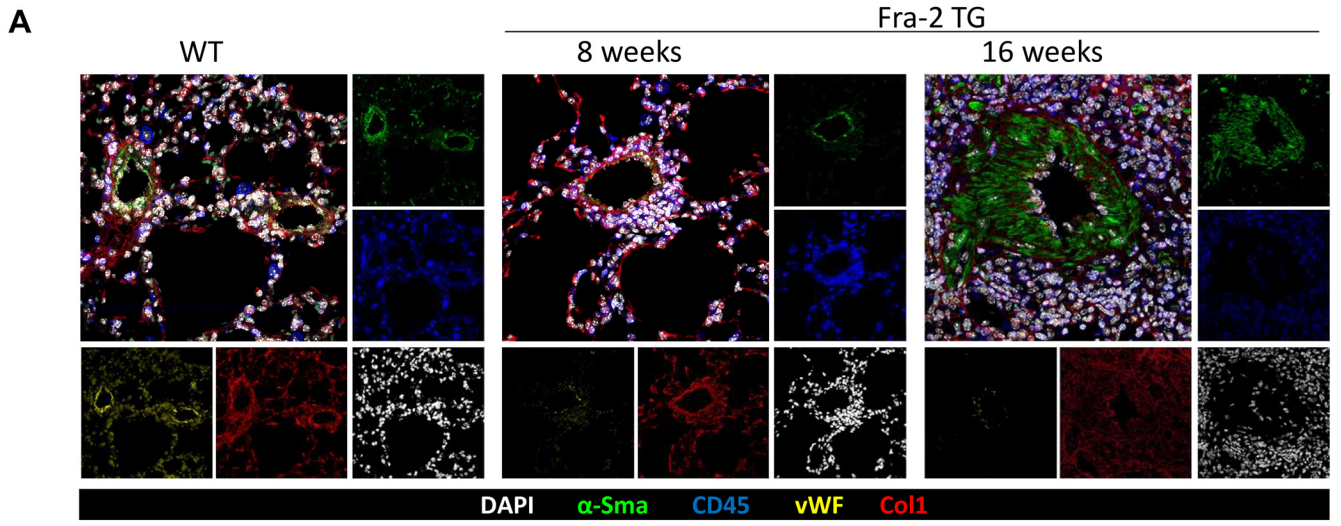

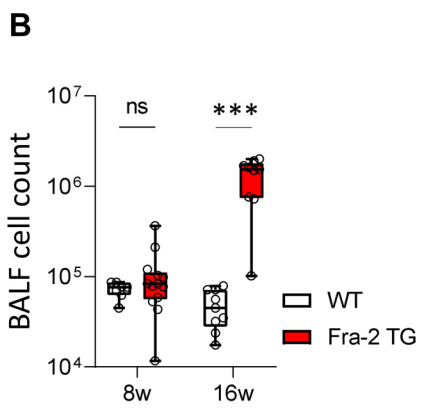

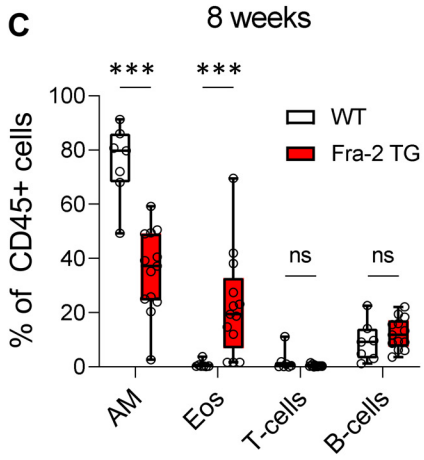

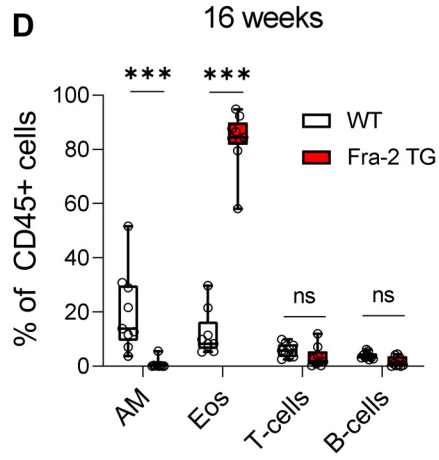

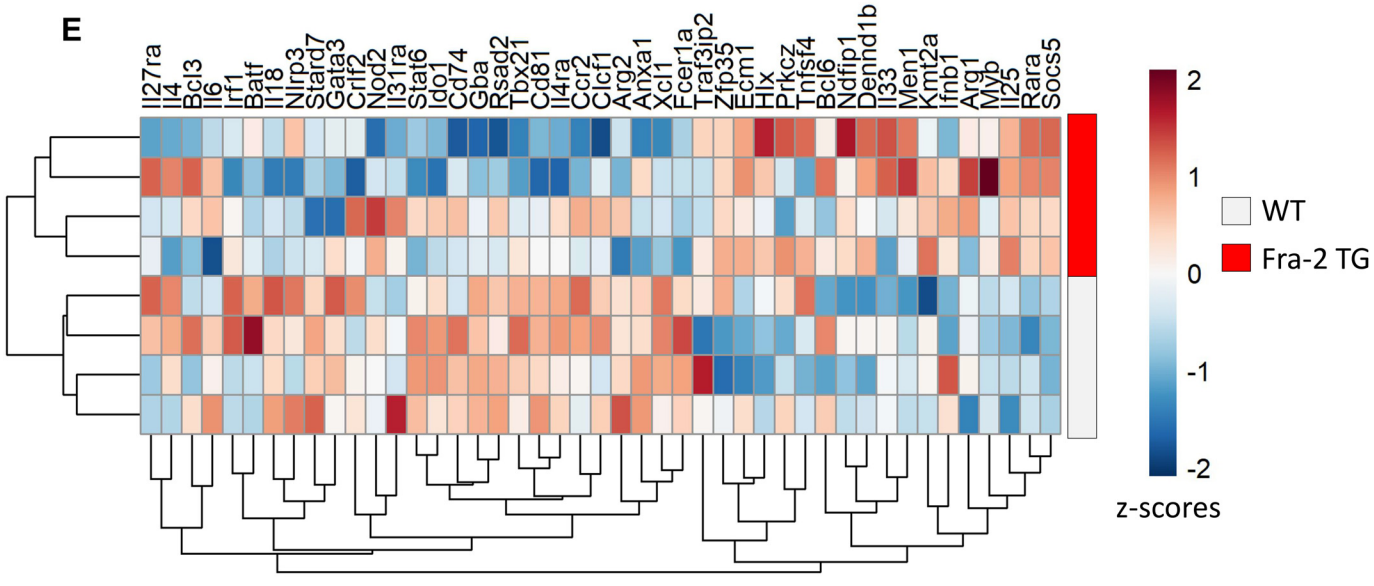

GO:0042092 type 2 immune response

AJP-Lung Cell Mol Physiol • doi:10.1152/ajplung.00274.2024 • www.ajplung.org

DISCUSSION

In our study presented here, we demonstrate for the first time that pulmonary arterial remodeling and hyperresponsiveness in Fra-2 TG mice are driven by proinflammatory signaling and involves pulmonary type 2 cytokine activity. Treatment with budesonide was able to completely halt the pulmonary vascular remodeling process in Fra-2 overexpressing mice, whereas IL-13 neutralizing antibodies partially alleviated it. Transcriptomic and flow cytometry analyses indicated an early shift toward type 2 inflammation in Fra-2 TG mice, which was reflected by the presence of type 2-predominant eosinophilic lung inflammation in Fra-2 TG mice, as shown previously (25, 30, 54).

Corroborating the contribution of type 2 inflammation to the development of PAH, lung-specific overexpression of IL-13 has been previously shown to lead to a PAH phenotype in mice (21). Similarly, mice challenged with ovalbumin, house dust-mite and *Schistosoma* developed a type 2-driven immune response along with varying degrees of pulmonary hypertension. Blocking IL-13 attenuated vascular remodeling in aspergillus-induced pulmonary hypertension (2, 5, 55). Also, pulmonary artery remodeling in mice coexposed to house dust mite and particulate matter was shown to be ameliorated by inhibiting IL-13 signaling via neutralization of IL-13 and IL-17 (22). Likewise, double-knockout mice of both type 2 cytokines IL-4 and IL-13 were found to be protected against pulmonary vascular disease after Schistosoma exposure (2). Depletion of $CD4^+$ T cells protects from antigen-induced pulmonary arterial remodeling, further pointing toward a causative interdependence.

The potential of targeted immune therapies to reverse established PAH requires further evaluation, as broad-based immunosuppressive treatments have only limited clinical benefit in most patients with PAH, except for those with systemic sclerosis and systemic lupus erythematosus (56).

In addition, other factors such as pulmonary vasoconstriction need to be considered. Indeed, vascular hyperresponsiveness was detected in Fra-2 TG mice, which potentiated the vasomotor response to hypoxia. Hypoxic pulmonary vasoconstriction (HPV) is a physiological mechanism to optimize ventilation-perfusion matching. HPV is believed to promote pulmonary hypertension in lung diseases associated with chronic hypoxia (40, 57–59). Here, we show for the first time that the pressure response to hypoxic ventilation is strongly increased in Fra-2 TG mice. Furthermore, vascular responses to other vasoconstrictive stimuli such as serotonin, the thromboxane analog U-46619, or potassium chloride were augmented in Fra-2 TG mice, indicating stimulus-unspecific pulmonary vascular hyperresponsiveness, which may point to a direct involvement of Fra-2 in the regulation of pulmonary vasoconstriction. This is corroborated by our in vitro data showing increased expression of genes involved in activation of the contractile apparatus, such as Rho GTPases RhoA and RhoB or Rho-Kinase 1 and -2 (ROCK1/2) following Fra-2 overexpression. In addition, Fra-2 overexpression together with IL-13 stimulation led to an increase in intracellular calcium without any contractile stimulus, pointing toward an interaction of Fra-2 activity and type 2 inflammation and a concomitant contractile status of PASMCs as seen in the vasculature of Fra-2 TG mice.

The increased mass of PASMCs in pulmonary vessels of Fra-2 TG mice could be an additional cause for higher contractility, irrespective of the contractile stimulus. In our in vitro experiments we did not detect increased PASMC proliferation due to Fra-2 overexpression. As Fra-2 is dependent on a dimerization partner carrying a transactivation domain, we cannot exclude that the lack of proliferation in vitro is due to a missing dimerization partner. One report highlighted a role of Fra-2 in smooth muscle cell differentiation (60). In contrast, another study reports increased myofibroblast differentiation in mice overexpressing Fra-2 specifically in α-SMA^+ cells (61). Whether augmented SMC differentiation in Fra-2 TG mice is involved in increased SMC mass in the vasculature of Fra-2 TG mice still needs to be determined.

Both type 2-specific lung inflammation (15, 17, 18) and *Nos3/eNOS* deficiency (62) are known to induce pulmonary vascular hyperresponsiveness. Although no downregulation of *Nos3/eNOS* was detected in the lungs of Fra-2 TG mice, levels of *Arg1*, a key enzyme in arginine metabolism, were highly upregulated. Transcriptome profiling revealed that the arginine metabolism imbalance is already present in young mice. This may be a direct effect of the pulmonary type 2 inflammation in Fra-2 TG mice observed here. Cho et al. (21) demonstrated that IL-13 overexpressing mice spontaneously developed a pulmonary hypertension phenotype at 2 mo of age with increased expression and activity of *Arg2*. Mechanistically, this results in substrate competition of arginases and eNOS and therefore decreased NO production and bioavailability (21). Moreover, *Arg2* deficiency in IL-13 TG mice diminished pulmonary arterial remodeling and right ventricular systolic pressure, whereas NO synthesis was increased. Consistent with this hypothesis, our results presented here show a decrease in NO bioavailability in the lung tissue of Fra-2 TG mice. The lack of this important vasodilator could therefore contribute to pre-constriction and vascular hyperresponsiveness in Fra-2 TG mice (21, 63). Thus, decreased NO availability due to L-arginine metabolism imbalance as well as IL-13/Fra-2 synergisms seem to contribute to the observed hyperresponsiveness of the pulmonary vasculature in Fra-2 TG.

In line with our data showing an imbalanced L-arginine metabolism and muscularization of formerly nonmuscularized

Figure 4. Fra-2 transgenic mice exhibit perivascular, type 2-predominant/eosinophilic inflammation. *A*: representative multicolor immunofluorescence images of endothelium (von Willebrand factor = vWF, yellow), smooth muscle cells (α-smooth muscle actin = α-SMA, green), inflammatory cells ($CD45^+$, blue), collagen type I (Col1, red), and nuclei (DAPI, white) staining. *B*: inflammatory cell counts in the bronchoalveolar lavage fluid (BALF) of Fra-2 TG and WT mice at the age of 8 and 16 wk. *C* and *D*: relative proportion of alveolar macrophages (AM), eosinophils (Eos), T cells, and B cells in the BALF of Fra-2 TG and WT control mice at the age of 8 wk (*C*) and 16 wk (*D*). *B–D*: two-way ANOVA with Sidak's multiple comparisons test, $^{***}P < 0.001$. Each datapoint represents one animal. *E*: transcriptome analysis of lung homogenates of 8-wk-old Fra-2 TG or WT mice ($n = 4$): heatmap with unbiased hierarchical clustering of genes annotated to the gene ontology "type 2 immune response" (GO:0042092), z-scores are shown. Fra-2, Fos-related antigen-2; ns, not significant; TG, transgenic; WT, wildtype.

lung vessels in 8-wk-old Fra-2 TG mice, an elevated RVSP was already detectable at this time point (26). By redirecting L-arginine metabolism, *Arg1/2* not only interferes with NO production and subsequently NO bioavailability but also increases the formation of polyamines and L-proline, important compounds in collagen synthesis and SMC growth (64). As a result, altered L-arginine metabolism in Fra-2 TG mice likely not only contributes to vascular hyperresponsiveness but also to pulmonary vascular remodeling and collagen deposition.

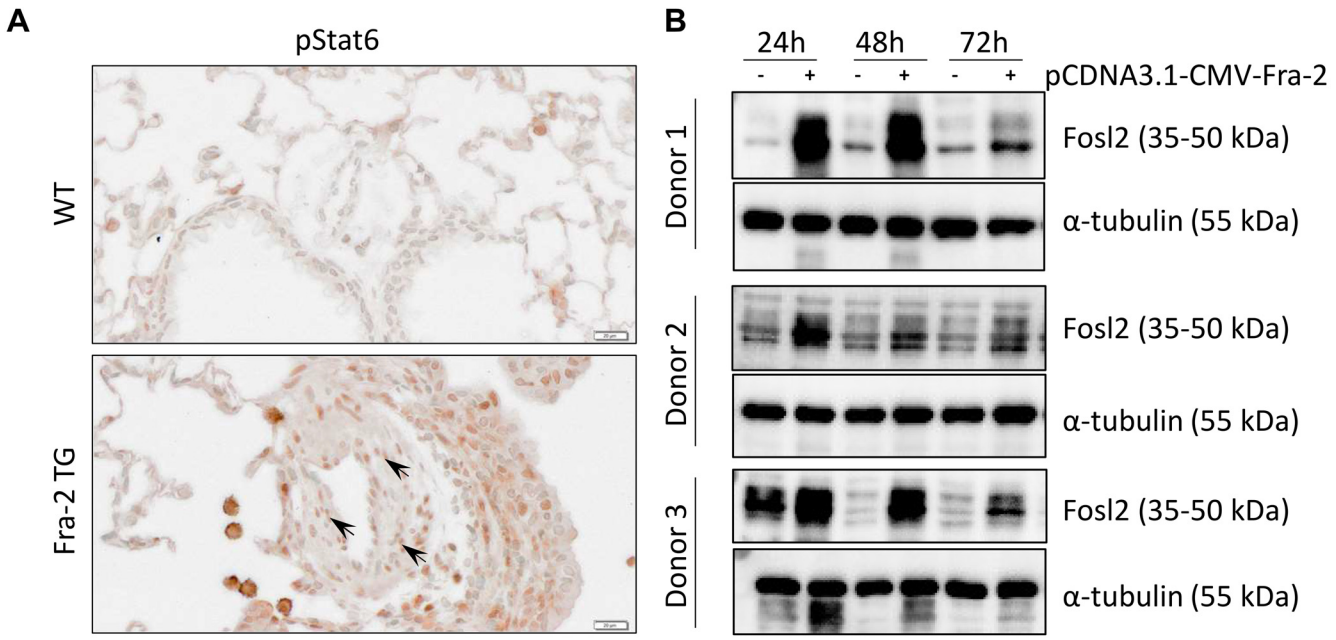

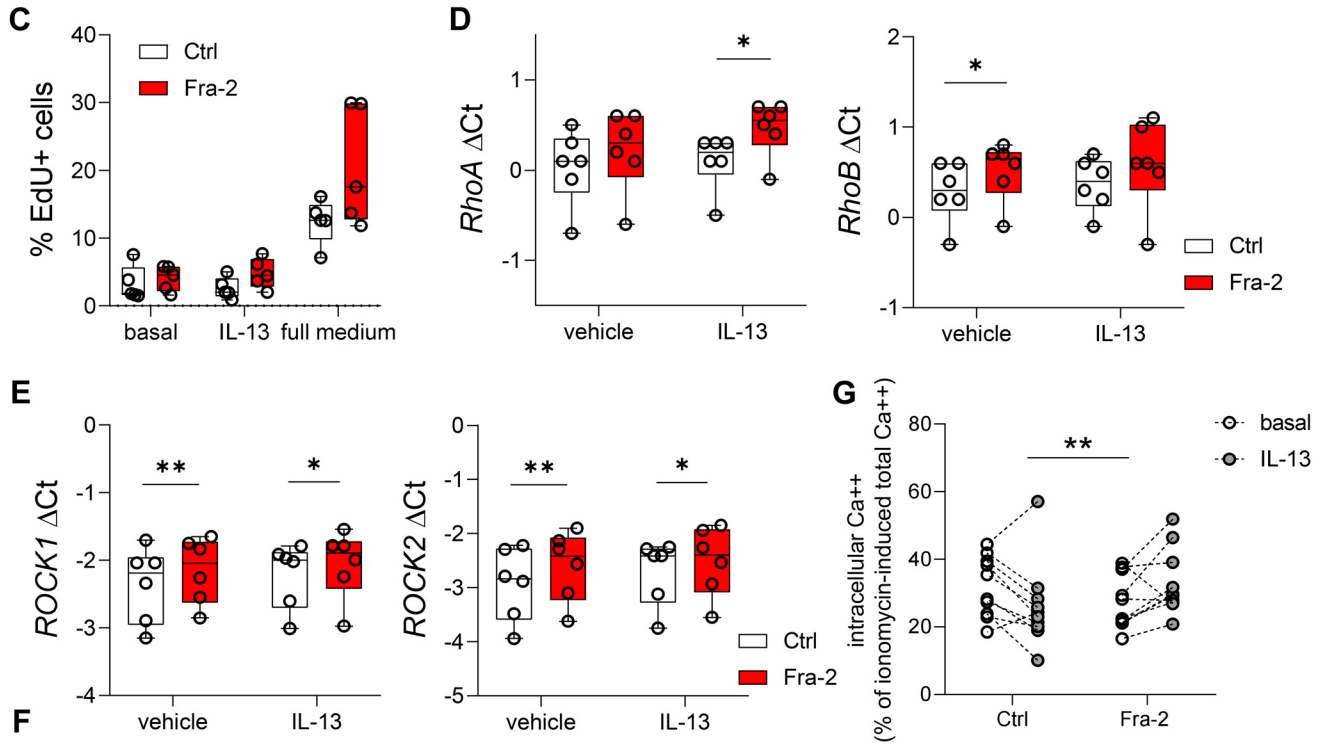

F

	RhoA		RhoB		ROCK1		ROCK2	
Source of Variation	%	P value	%	P value	%	P value	%	P value
Interaction	1.462	0.261	0.01337	0.8759	0.05981	0.4296	0.3393	0.0976
Fra-2 overexpression	13.15	**0.0188**	9.747	**0.0256**	3.897	**0.0471**	4.72	**0.0431**
IL-13 treatment	4.36	**0.0388**	1.083	0.3124	1.582	0.1174	1.713	0.1534

Source of Variation	% of total variation	P value	P value summary
Interaction	8.726	0.0071	**
Fra-2 overexrpression	0.3921	0.7607	ns
IL-13 treatment	0.00756	0.9298	ns
Subjects (matching)	73.84	0.0016	**

AJP-Lung Cell Mol Physiol • doi:10.1152/ajplung.00274.2024 • www.ajplung.org

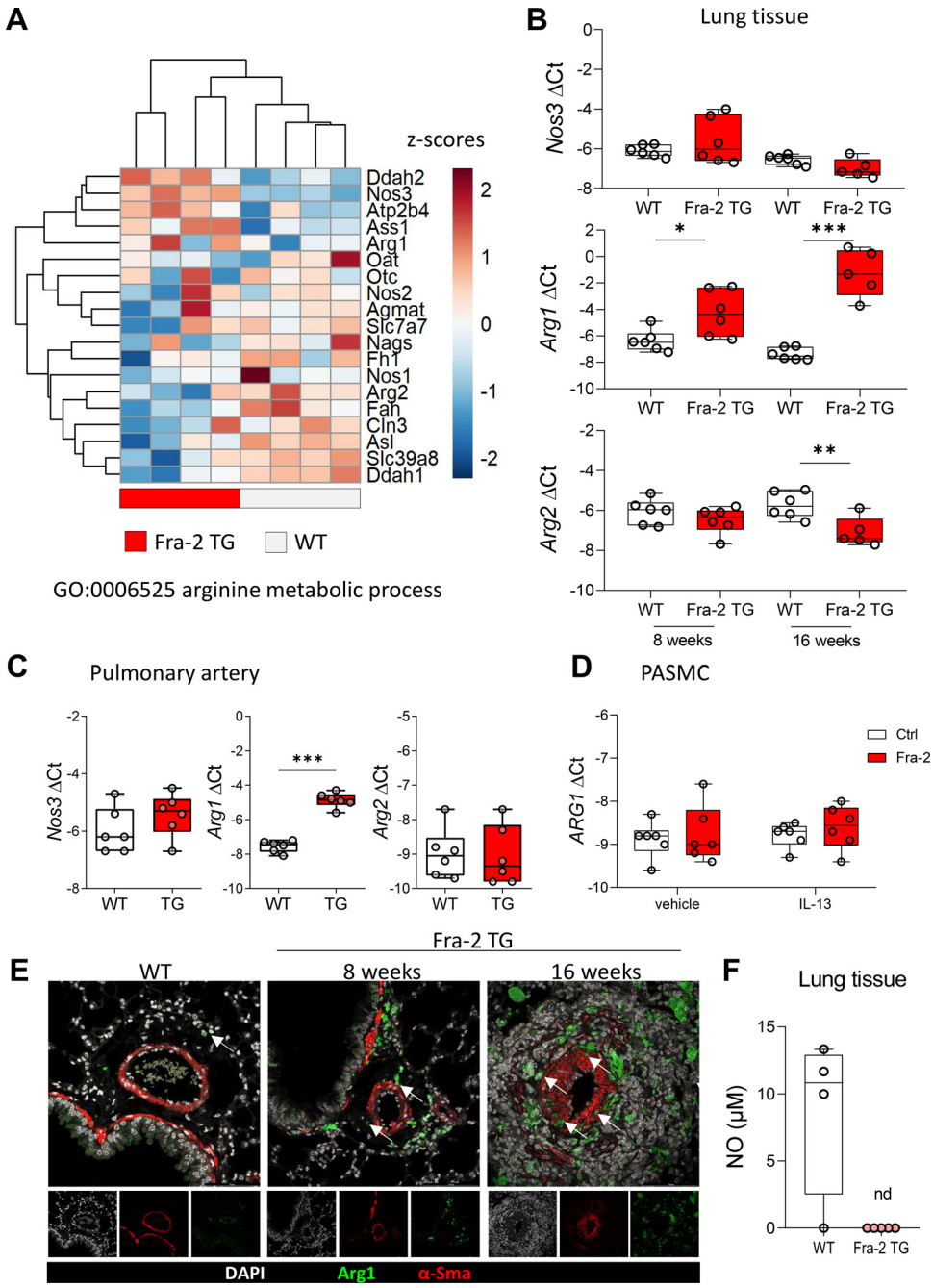

Figure 6. Dysbalance of arginine metabolism in Fra-2 transgenic mice. *A*: transcriptome analysis of lung homogenates of 8-wk-old Fra-2 transgenic (TG) or wild-type (WT) mice ($n = 4$ animals/group): heatmap with hierarchical clustering of genes annotated to the gene ontology "arginine metabolic process" (GO: 0006525), *z*-scores are shown. *B* and *C*: relative gene expression levels of endothelial nitric oxide synthase (*Nos3/eNos*), arginase 1 and 2 (*Arg1/Arg2*) in lung homogenates (*B*) of 8- and 16-wk-old Fra-2 TG and WT control mice an pulmonary arteries (*C*) of 16-wk-old Fra-2 TG and WT mice. Unpaired *t* test, $^{*}P < 0.05$, $^{**}P < 0.01$, $^{***}P < 0.001$. Each datapoint represents one animal. *D*: *ARG1* gene expression in PASMC following Fra-2 overexpression and IL-13 stimulation ($n = 6$ technical replicates from 4 different donor cells). *E*: multicolor immunofluorescence images of smooth muscle cells (α-smooth muscle actin = α-SMA, red), arginase 1 (green), and nuclei (DAPI, white) staining. White arrows indicate Arg1-positive cells in the vicinity of and within the vessel wall. *F*: NO levels measured in lung tissue homogenates of 16-wk-old Fra-2 TG ($n = 5$) and WT ($n = 4$) mice. Fra-2, Fos-related antigen-2.

In summary, increased vascular hyperresponsiveness in Fra-2 TG mice is most likely elicited by two factors. First, the PASMC intrinsic contractile status due to the presence of Fra-2 and second, the imbalanced arginine metabolism due to arginase-expressing immune cells surrounding and infiltration the pulmonary artery vessel wall.

This study is limited by the analysis of only female mice in one mouse model, use of archived tissue samples with a

Figure 5. Effects of interleukin (IL)-13 and Fra-2 overexpression on proliferation and intracellular calcium of pulmonary artery smooth muscle cells. *A*: immunohistochemical staining of IL-13 downstream signaling molecule pStat6 in the pulmonary vasculature in Fra-2 transgenic (TG) and wild-type (WT) mice. Arrows indicate intranuclear pStat6 staining in the vascular smooth muscle cell layer of Fra-2 TG mice. *B*: Fra-2 overexpression in PASMCs after 24, 48, and 72 h as determined by Western blot analysis. Alpha-tubulin served as a loading control. *C*: proliferation of PASMCs with and without Fra-2 overexpression in basal medium (0% FCS), with IL-13 stimulation or in full medium (including 5% FCS). Each datapoint represents one measurement. In total, six technical replicates from four different donor cells were measured. *D* and *E*: expression levels of *RhoA*, *RhoB*, *ROCK1*, and *ROCK2* in PASMCs following Fra-2 overexpression and stimulation with IL-13. Two-way ANOVA with Sidak's multiple comparison test, $^{*}P < 0.05$, $^{**}P < 0.01$. Each datapoint represents one measurement. In total, six technical replicates from four different donor cells were measured. *F*: results of two-way ANOVA analysis of *D* and *E*. *G*: intracellular Ca^{++} in primary human PASMCs following Fra-2 overexpression and IL-13 (10 ng/mL for 24 h) treatment. Two-way ANOVA, $^{**}P < 0.01$. Fra-2, Fos-related antigen-2; PASMC, pulmonary arterial smooth muscle cell.

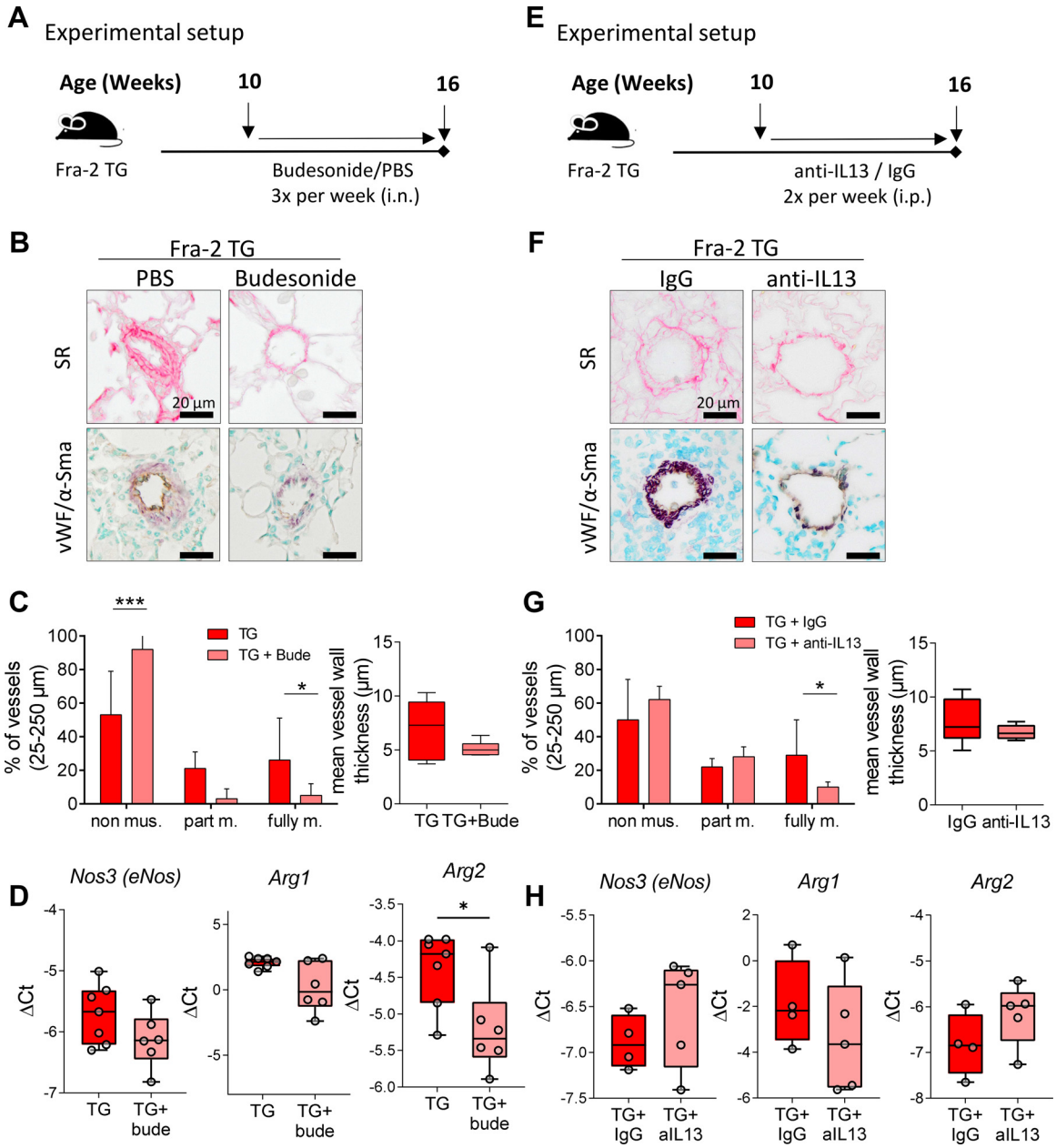

Figure 7. Anti-inflammatory treatment using glucocorticosteroids or type 2-specific anti-IL-13 blocking antibodies (partially) ameliorates vascular remodeling in the Fra-2 transgenic mouse model of SSc-PAH. *A*: schematic representation of intranasal (i.n.) treatment with the glucocorticosteroid budesonide (bude) or PBS as control in Fra-2 transgenic (TG) mice. *B*: collagen (picrosirius red, SR) and von Willebrand factor (vWF)/α-smooth muscle actin (α-SMA) double staining of pulmonary vessels of Fra-2 TG mice with budesonide ($n = 6$) or PBS ($n = 7$) treatment. *C*: quantification of muscularization of small pulmonary vessels (25–250 µm diameter). Non-m., non-muscularized, part m., partially muscularized, fully m., fully muscularized. Two-way ANOVA with Sidak's multiple comparison test, $^*P < 0.05$, $^{***}P < 0.001$. *D*: relative gene expression levels of endothelial nitric oxide synthase (*Nos3/eNos*), arginase 1 and 2 (*Arg1/Arg2*) in lung tissue of Fra-2 TG mice with ($n = 6$) or without ($n = 7$) budesonide treatment. Unpaired *t* test, $^*P < 0.0201$. *E*: schematic representation of intraperitoneal (ip) treatment with IL-13 neutralizing (anti-IL-13) antibodies or IgG isotype controls in Fra-2 TG mice. *F*: collagen (picrosirius red, SR) and vWF/α-SMA double staining of pulmonary vessels in Fra-2 TG mice with anti-IL-13 treatment ($n = 6$) or IgG treatment ($n = 7$). *G*: quantification of muscularization of small pulmonary vessels (25–250 µm diameter). Non-m., non-muscularized, part m., partially muscularized, fully m., fully muscularized. Two-way ANOVA with Sidak's multiple comparison test, $^*P < 0.05$. *H*: relative gene expression levels of endothelial nitric oxide synthase (*Nos3/eNos*), arginase 1 and 2 (*Arg1/Arg2*) in lung tissue of Fra-2 TG mice with ($n = 5$) and without ($n = 4$) anti-IL-13 treatment. Fra-2, Fos-related antigen-2.

limited number, and therefore low statistical power. However, we performed for the first time in vivo cardiac MRI measurements in Fra-2 TG mice and found signs of right ventricular hypertrophy, a significant increase in end-systolic right ventricular volume, and a decrease in right ventricular EF in 16-wk-old Fra-2 TG mice, reflecting right ventricular maladaptation similar to the human situation in patients with PAH (65, 66). Therefore, the presented data here on early vascular alterations with concomitant changes in PA blood flow and right ventricular function highlight once again the translational value of the Fra-2 TG model and the clinical relevance of the here presented data.

In conclusion, pulmonary hypertension in the Fra-2 TG mouse model of SSc-PAH is most likely multifactorial, conjointly elicited by type 2 inflammation, increased vasoconstriction, and progressive pulmonary arterial remodeling. This could have important clinical implications, as combination therapy targeting each of these mechanisms might be necessary to treat lung involvement in this deadly disease successfully. However, the current lack of clinical studies on type 2-specific anti-inflammatory treatments in patients with PAH underscores the need for further investigation in this promising area.

DATA AVAILABILITY

Data will be made available upon reasonable request.

SUPPLEMENTAL MATERIAL

Supplemental Fig. S1: https://doi.org/10.6084/m9.figshare.28069967.

Supplemental Table S1: https://doi.org/10.6084/m9.figshare.28069970.

ACKNOWLEDGMENTS

We thank Thomas Fuchs, Julia Kohlbacher, Kerstin Schweighofer, and Aisa Buko for excellent technical assistance. We are grateful to the Institute for Molecular Pathology Vienna and Prof. Erwin Wagner for Fra-2 TG mice and Fra-2/Control overexpression plasmids. K.A. acknowledges the use of DeepL Write for enhancing writing precision; the authors take full responsibility for the content of the publication.

GRANTS

M.W. was supported by the Deutsche Forschungsgemeinschaft (DFG; German Research Foundation)—SFB-1449 (project ID 431232613), sub-project B02 and SFB-TR84 (project ID 114933180), sub-projects C06 and C09, by the German Federal Ministry of Education and Research (BMBF) in the framework of e:Med CAPSyS (01ZX1604B and 01ZX1304B), PROVID (01KI20160A), e:Med SYMPATH (01ZX2206A and 01ZX1906A), NUM-NAPKON (01KX2121 and 01KX2021), Phage4Cure (16GW0141), MAPVAP (01KI2124), PulmVasC (01EP2102B), and CAP-TSD (031L0286B). V.B. was supported by the Austrian Science Foundation (FWF; T1032-B34). L.M.M. received funding from Austrian Science Fund (FWF) (KLI 884-B). A.B. received funding from the European Respiratory Society (short-term research travel fellowship 2015, grant 9543) and the Austrian Society of Pneumology (short-term fellowship 2015).

DISCLOSURES

C.T. received funding for research from Deutsche Gesellschaft für Pneumologie und Beatmungsmedizin e. V., Bayer HealthCare, Boehringer Ingelheim, and for lectures and advisory from Actelion Pharmaceuticals, AstraZeneca, Berlin-Chemie, Boehringer Ingelheim, GlaxoSmithKline, and for nonfinancial support from Actelion, ALK-Abelló, Bayer HealthCare, Boehringer Ingelheim, and GlaxoSmithKline. None of the other authors has any conflicts of interest, financial or otherwise, to disclose.

AUTHOR CONTRIBUTIONS

A.B., C.T., and G.K. conceived and designed research; A.B., V.B., P.P.J., G.K., E.B., and C.N. performed experiments; A.B., V.B., P.P.J., G.K., J.W., M.W., L.M.M., C.T., and G.K. analyzed data; A.B., V.B., J.W., M.W., L.M.M., C.T., and G.K. interpreted results of experiments; A.B. and C.T. prepared figures; A.B., K.A., C.T., and G.K. drafted manuscript; A.B., V.B., P.P.J., G.K., E.B., J.W., K.A., C.N., A.O., M.W., S.C., L.M.M., C.T., and G.K. edited and revised manuscript; A.B., V.B., P.P.J., G.K., E.B., J.W., K.A., C.N., A.O., M.W., S.C., L.M.M., C.T., and G.K. approved final version of manuscript.

REFERENCES

1. **Tuder RM.** Pulmonary vascular remodeling in pulmonary hypertension. *Cell Tissue Res* 367: 643–649, 2017. doi:10.1007/s00441-016-2539-y.
2. **Kumar R**, **Mickael C**, **Chabon J**, **Gebreab L**, **Rutebemberwa A**, **Garcia AR**, **Koyanagi DE**, **Sanders L**, **Gandjeva A**, **Kearns MT**, **Barthel L**, **Janssen WJ**, **Mauad T**, **Bandeira A**, **Schmidt E**, **Tuder RM**, **Graham BB.** The causal role of IL-4 and IL-13 in Schistosoma mansoni pulmonary hypertension. *Am J Respir Crit Care Med* 192: 998–1008, 2015. doi:10.1164/rccm.201410-1820OC.
3. **Höppner J**, **Tabeling C**, **Casteleyn V**, **Kedor C**, **Windisch W**, **Burmester GR**, **Huscher D**, **Siegert E.** Comprehensive autoantibody profiles in systemic sclerosis: clinical cluster analysis. *Front Immunol* 13: 1045523, 2023. doi:10.3389/fimmu.2022.1045523.
4. **Becker MO**, **Kill A**, **Kutsche M**, **Guenther J**, **Rose A**, **Tabeling C**, **Witzenrath M**, **Kühl AA**, **Heidecke H**, **Ghofrani HA**, **Tiede H**, **Schermuly RT**, **Nickel N**, **Hoeper MM**, **Lukitsch I**, **Gollasch M**, **Kuebler WM**, **Bock S**, **Burmester GR**, **Dragun D**, **Riemekasten G.** Vascular receptor autoantibodies in pulmonary arterial hypertension associated with systemic sclerosis. *Am J Respir Crit Care Med* 190: 808–817, 2014. doi:10.1164/rccm.201403-0442OC.
5. **Daley E**, **Emson C**, **Guignabert C**, **de Waal Malefyt R**, **Louten J**, **Kurup VP**, **Hogaboam C**, **Taraseviciene-Stewart L**, **Voelkel NF**, **Rabinovitch M**, **Grunig E**, **Grunig G.** Pulmonary arterial remodeling induced by a Th2 immune response. *J Exp Med* 205: 361–372, 2008. doi:10.1084/jem.20071008.
6. **Archer SL**, **Weir EK**, **Wilkins MR.** Basic science of pulmonary arterial hypertension for clinicians. *Circulation* 121: 2045–2066, 2010. doi:10.1161/CIRCULATIONAHA.108.847707.
7. **Rajagopal K**, **Bryant AJ**, **Sahay S**, **Wareing N**, **Zhou Y**, **Pandit LM**, **Karmouty-Quintana H.** Idiopathic pulmonary fibrosis and pulmonary hypertension: heracles meets the Hydra. *Br J Pharmacol* 178: 172–186, 2021. doi:10.1111/bph.15036.
8. **Goldenberg NM**, **Rabinovitch M**, **Steinberg BE.** Inflammatory basis of pulmonary arterial hypertension. *Anesthesiology* 131: 898–907, 2019. doi:10.1097/ALN.0000000000002740.
9. **Le Pavec J**, **Humbert M**, **Mouthon L**, **Hassoun PM.** Systemic sclerosis-associated pulmonary arterial hypertension. *Am J Respir Crit Care Med* 181: 1285–1293, 2010. doi:10.1164/rccm.200909-1331PP.
10. **Morrisroe K**, **Stevens W**, **Huq M**, **Prior D**, **Sahhar J**, **Ngian G-S**, **Celermajer D**, **Zochling J**, **Proudman S**, **Nikpour M**; **Australian Scleroderma Interest Group (ASIG).** Survival and quality of life in incident systemic sclerosis-related pulmonary arterial hypertension. *Arthritis Res Ther* 19: 122, 2017. doi:10.1186/s13075-017-1341-x.
11. **Maron BA**, **Leopold JA**, **Hemnes AR.** Metabolic syndrome, neurohumoral modulation, and pulmonary arterial hypertension. *Br J Pharmacol* 177: 1457–1471, 2020. doi:10.1111/bph.14968.
12. **Wang AP**, **Yang F**, **Tian Y**, **Su JH**, **Gu Q**, **Chen W**, **Gong SX**, **Ma XF**, **Qin XP**, **Jiang ZS.** Pulmonary artery smooth muscle cell senescence promotes the proliferation of PASMCs by paracrine IL-6 in hypoxia-induced pulmonary hypertension. *Front Physiol* 12: 656139, 2021. doi:10.3389/fphys.2021.656139.
13. **Rabinovitch M**, **Guignabert C**, **Humbert M**, **Nicolls MR.** Inflammation and immunity in the pathogenesis of pulmonary arterial hypertension. *Circ Res* 115: 165–175, 2014. doi:10.1161/CIRCRESAHA.113.301141.
14. **Marsh LM**, **Jandl K**, **Grünig G**, **Foris V**, **Bashir M**, **Ghanim B**, **Klepetko W**, **Olschewski H**, **Olschewski A**, **Kwapiszewska G.** The inflammatory cell landscape in the lungs of patients with idiopathic pulmonary arterial hypertension. *Eur Respir J* 51: 1701214, 2018. doi:10.1183/13993003.01214-2017.

15. **Tabeling C**, **González Calera CR**, **Lienau J**, **Höppner J**, **Tschernig T**, **Kershaw O**, **Gutbier B**, **Naujoks J**, **Herbert J**, **Opitz B**, **Gruber AD**, **Hocher B**, **Suttorp N**, **Heidecke H**, **Burmester G-R**, **Riemekasten G**, **Siegert E**, **Kuebler WM**, **Witzenrath M.** Endothelin B receptor immunodynamics in pulmonary arterial hypertension. *Front Immunol* 13: 895501, 2022. doi:10.3389/fimmu.2022.895501.
16. **Mattoo H**, **Bangari DS**, **Cummings S**, **Humulock Z**, **Habiel D**, **Xu EY**, **Pate N**, **Resnick R**, **Savova V**, **Qian G**, **Beil C**, **Rao E**, **Nestle FO**, **Bryce PJ**, **Subramaniam A.** Molecular features and stages of pulmonary fibrosis driven by type 2 inflammation. *Am J Respir Cell Mol Biol* 69: 404–421, 2023. doi:10.1165/rcmb.2022-0301OC.
17. **Haberberger RV**, **Tabeling C**, **Runciman S**, **Gutbier B**, **König P**, **Andratsch M**, **Schütte H**, **Suttorp N**, **Gibbins I**, **Witzenrath M.** Role of sphingosine kinase 1 in allergen-induced pulmonary vascular remodeling and hyperresponsiveness. *J Allergy Clin Immunol* 124: 933–941.e1-9, 2009. doi:10.1016/j.jaci.2009.06.034.
18. **Witzenrath M**, **Ahrens B**, **Kube SM**, **Hocke AC**, **Rosseau S**, **Hamelmann E**, **Suttorp N**, **Schütte H.** Allergic lung inflammation induces pulmonary vascular hyperresponsiveness. *Eur Respir J* 28: 370–377, 2006. doi:10.1183/09031936.06.00080105.
19. **Gomez-Arroyo J**, **Saleem SJ**, **Mizuno S**, **Syed AA**, **Bogaard HJ**, **Abbate A**, **Taraseviciene-Stewart L**, **Sung Y**, **Kraskauskas D**, **Farkas D**, **Conrad DH**, **Nicolls MR**, **Voelkel NF.** A brief overview of mouse models of pulmonary arterial hypertension: problems and prospects. *Am J Physiol Lung Cell Mol Physiol* 302: L977–L991, 2012. doi:10.1152/ajplung.00362.2011.
20. **Mushaben EM**, **Hershey GK**, **Pauciulo MW**, **Nichols WC**, **Le Cras TD.** Chronic allergic inflammation causes vascular remodeling and pulmonary hypertension in Bmpr2 hypomorph and wild-type mice. *PLoS One* 7: e32468, 2012. doi:10.1371/journal.pone.0032468.
21. **Cho WK**, **Lee CM**, **Kang MJ**, **Huang Y**, **Giordano FJ**, **Lee PJ**, **Trow TK**, **Homer RJ**, **Sessa WC**, **Elias JA**, **Lee CG.** IL-13 receptor α_2 -arginase 2 pathway mediates IL-13-induced pulmonary hypertension. *Am J Physiol Lung Cell Mol Physiol* 304: L112–L124, 2013. doi:10.1152/ajplung.00101.2012.
22. **Park S**, **Chen W**, **Esmaeil N**, **Lucas B**, **Marsh LM**, **Reibman J**, **Grunig G.** Interleukin 13– and interleukin 17A–induced pulmonary hypertension phenotype due to inhalation of antigen and fine particles from air pollution. *Pulm Circ* 4: 654–668, 2014. doi:10.1086/678511.
23. **Eferl R**, **Hasselblatt P**, **Rath M**, **Popper H**, **Zenz R**, **Komnenovic V**, **Idarraga MH**, **Kenner L**, **Wagner EF.** Development of pulmonary fibrosis through a pathway involving the transcription factor Fra-2/AP-1. *Proc Natl Acad Sci USA* 105: 10525–10530, 2008. doi:10.1073/pnas.0801414105.
24. **Biasin V**, **Crnkovic S**, **Sahu-Osen A**, **Birnhuber A**, **El Agha E**, **Sinn K**, **Klepetko W**, **Olschewski A**, **Bellusci S**, **Marsh LM**, **Kwapiszewska G.** PDGFRα and αSMA mark two distinct mesenchymal cell populations involved in parenchymal and vascular remodeling in pulmonary fibrosis. *Am J Physiol Lung Cell Mol Physiol* 318: L684–L697, 2020. doi:10.1152/ajplung.00128.2019.
25. **Birnhuber A**, **Crnkovic S**, **Biasin V**, **Marsh LM**, **Odler B**, **Sahu-Osen A**, **Stacher-Priehse E**, **Brcic L**, **Schneider F**, **Cikes N**, **Ghanim B**, **Klepetko W**, **Graninger W**, **Allanore Y**, **Eferl R**, **Olschewski A**, **Olschewski H**, **Kwapiszewska G.** IL-1 receptor blockade skews inflammation towards Th2 in a mouse model of systemic sclerosis. *Eur Respir J* 54: 1900154, 2019. doi:10.1183/13993003.00154-2019.
26. **Biasin V**, **Marsh LM**, **Egemnazarov B**, **Wilhelm J**, **Ghanim B**, **Klepetko W**, **Wygrecka M**, **Olschewski H**, **Eferl R**, **Olschewski A**, **Kwapiszewska G.** Meprin β, a novel mediator of vascular remodelling underlying pulmonary hypertension. *J Pathol* 233: 7–17, 2014. doi:10.1002/path.4303.
27. **Birnhuber A**, **Jandl K**, **Biasin V**, **Fließer E**, **Valzano F**, **Marsh LM**, **Krolczik C**, **Olschewski A**, **Wilhelm J**, **Toller W**, **Heinemann A**, **Olschewski H**, **Wygrecka M**, **Kwapiszewska G.** Pirfenidone exacerbates Th2-driven vasculopathy in a mouse model of systemic sclerosis-associated interstitial lung disease. *Eur Respir J* 60: 2102347, 2022. doi:10.1183/13993003.02347-2021.
28. **Reich N**, **Maurer B**, **Akhmetshina A**, **Venalis P**, **Dees C**, **Zerr P**, **Palumbo K**, **Zwerina J**, **Nevskaya T**, **Gay S**, **Distler O**, **Schett G**, **Distler JH.** The transcription factor Fra-2 regulates the production of extracellular matrix in systemic sclerosis. *Arthritis Rheum* 62: 280–290, 2010. doi:10.1002/art.25056.
29. **Maurer B**, **Busch N**, **Jüngel A**, **Pileckyte M**, **Gay RE**, **Michel BA**, **Schett G**, **Gay S**, **Distler J**, **Distler O.** Transcription factor Fos-related antigen-2 induces progressive peripheral vasculopathy in mice closely resembling human systemic sclerosis. *Circulation* 120: 2367–2376, 2009. doi:10.1161/CIRCULATIONAHA.109.855114.
30. **Birnhuber A**, **Biasin V**, **Schnoegl D**, **Marsh LM**, **Kwapiszewska G.** Transcription factor Fra-2 and its emerging role in matrix deposition, proliferation and inflammation in chronic lung diseases. *Cell Signal* 64: 109408, 2019. doi:10.1016/j.cellsig.2019.109408.
31. **Gungl A**, **Biasin V**, **Wilhelm J**, **Olschewski A**, **Kwapiszewska G**, **Marsh LM.** Fra2 overexpression in mice leads to non-allergic asthma development in an IL-13 dependent manner. *Front Immunol* 9: 2018, 2018. doi:10.3389/fimmu.2018.02018.
32. **Frantz C**, **Cauvet A**, **Durand A**, **Gonzalez V**, **Pierre R**, **Do Cruzeiro M**, **Bailly K**, **Andrieu M**, **Orvain C**, **Avouac J**, **Ottaviani M**, **Thuillet R**, **Tu L**, **Guignabert C**, **Lucas B**, **Auffray C**, **Allanore Y.** Driving role of interleukin-2–related regulatory CD4+ T cell deficiency in the development of lung fibrosis and vascular remodeling in a mouse model of systemic sclerosis. *Arthritis Rheumatol* 74: 1387–1398, 2022. doi:10.1002/art.42111.
33. **Kwiatkowski G**, **Czyzynska-Cichon I**, **Tielemans B**, **Geerkens L**, **Jasztal A**, **Velde GV**, **Chłopicki S.** Retrospectively gated ultrashort-echo-time MRI T_1 mapping reveals compromised pulmonary microvascular NO-dependent function in a murine model of acute lung injury. *NMR Biomed* 37: e5105, 2024. doi:10.1002/nbm.5105.
34. **Schneider CA**, **Rasband WS**, **Eliceiri KW.** NIH Image to ImageJ: 25 years of image analysis. *Nat Methods* 9: 671–675, 2012. doi:10.1038/nmeth.2089.
35. **Ritchie ME**, **Phipson B**, **Wu D**, **Hu Y**, **Law CW**, **Shi W**, **Smyth GK.** limma powers differential expression analyses for RNA-sequencing and microarray studies. *Nucleic Acids Res* 43: e47, 2015. doi:10.1093/nar/gkv007.
36. **Hoffmann J**, **Wilhelm J**, **Marsh LM**, **Ghanim B**, **Klepetko W**, **Kovacs G**, **Olschewski H**, **Olschewski A**, **Kwapiszewska G.** Distinct differences in gene expression patterns in pulmonary arteries of patients with chronic obstructive pulmonary disease and idiopathic pulmonary fibrosis with pulmonary hypertension. *Am J Respir Crit Care Med* 190: 98–111, 2014. doi:10.1164/rccm.201401-0037OC.
37. **R Core Team.** R: A Language and Environment for Statistical Computing. Vienna, Austria: R Foundation for Statistical Computing, https://www.r-project.org/.
38. **Kolde R.** pheatmap: Pretty Heatmaps. R package version 1.0.12. https://cran.r-project.org/web/packages/pheatmap/index.html.
39. **Tabeling C**, **Herbert J**, **Hocke AC**, **Lamb DJ**, **Wollin SL**, **Erb KJ**, **Boiarina E**, **Movassagh H**, **Scheffel J**, **Doehn JM**, **Hippenstiel S**, **Maurer M**, **Gounni AS**, **Kuebler WM**, **Suttorp N**, **Witzenrath M.** Spleen tyrosine kinase inhibition blocks airway constriction and protects from Th2-induced airway inflammation and remodeling. *Allergy* 72: 1061–1072, 2017. doi:10.1111/all.13101.
40. **Nagaraj C**, **Tabeling C**, **Nagy BM**, **Jain PP**, **Marsh LM**, **Papp R**, **Pienn M**, **Witzenrath M**, **Ghanim B**, **Klepetko W**, **Weir EK**, **Heschl S**, **Kwapiszewska G**, **Olschewski A**, **Olschewski H.** Hypoxic vascular response and ventilation/perfusion matching in end-stage COPD may depend on p22phox. *Eur Respir J* 50: 1601651, 2017. doi:10.1183/13993003.01651-2016.
41. **Tabeling C**, **Noe E**, **Naujoks J**, **Doehn JM**, **Hippenstiel S**, **Opitz B**, **Suttorp N**, **Klopfleisch R**, **Witzenrath M.** PKCα deficiency in mice is associated with pulmonary vascular hyperresponsiveness to thromboxane A2 and increased thromboxane receptor expression. *J Vasc Res* 52: 279–288, 2015. doi:10.1159/000443402.
42. **Spöhr F**, **Busch CJ**, **Reich C**, **Motsch J**, **Gebhard MM**, **Kuebler WM**, **Bloch KD**, **Weimann J.** 4-Aminopyridine restores impaired hypoxic pulmonary vasoconstriction in endotoxemic mice. *Anesthesiology* 107: 597–604, 2007. doi:10.1097/01.anes.0000281897.13703.fd.
43. **Biasin V**, **Wygrecka M**, **Bärnthaler T**, **Jandl K**, **Jain P**, **Bálint Z**, **Kovacs G**, **Leitinger G**, **Kolb-Lenz D**, **Kornmueller K**, **Peters F**, **Sinn K**, **Klepetko W**, **Heinemann A**, **Olschewski A**, **Becker-Pauly C**, **Kwapiszewska G.** Docking of meprin α to heparan sulphate protects the endothelium from inflammatory cell extravasation. *Thromb Haemost* 118: 1790–1802, 2018. doi:10.1055/s-0038-1670657.
44. **Jain PP**, **Leber R**, **Nagaraj C**, **Leitinger G**, **Lehofer B**, **Olschewski H**, **Olschewski A**, **Prassl R**, **Marsh LM.** Liposomal nanoparticles encapsulating iloprost exhibit enhanced vasodilation in pulmonary arteries. *Int J Nanomedicine* 9: 3249–3261, 2014. doi:10.2147/IJN.S63190.
45. **Nagaraj C**, **Tang B**, **Nagy BM**, **Papp R**, **Jain PP**, **Marsh LM**, **Meredith AL**, **Ghanim B**, **Klepetko W**, **Kwapiszewska G**, **Weir EK**,

Olschewski H, **Olschewski A.** Docosahexaenoic acid causes rapid pulmonary arterial relaxation via KCa channel-mediated hyperpolarisation in pulmonary hypertension. *Eur Respir J* 48: 1127–1136, 2016. doi:10.1183/13993003.01814-2015.

46. **Hu R**, **Tousignant C**, **Chen R.** Flow velocity patterns in the pulmonary artery and pulmonary hypertension. *Can J Anaesth* 59: 716–719, 2012. doi:10.1007/s12630-012-9700-1.
47. **Thibault HB**, **Kurtz B**, **Raher MJ**, **Shaik RS**, **Waxman A**, **Derumeaux G**, **Halpern EF**, **Bloch KD**, **Scherrer-Crosbie M.** Noninvasive assessment of murine pulmonary arterial pressure: validation and application to models of pulmonary hypertension. *Circ Cardiovasc Imaging* 3: 157–163, 2010. doi:10.1161/CIRCIMAGING.109.887109.
48. **Dabestani A**, **Mahan G**, **Gardin JM**, **Takenaka K**, **Burn C**, **Allfie A**, **Henry WL.** Evaluation of pulmonary artery pressure and resistance by pulsed Doppler echocardiography. *Am J Cardiol* 59: 662–668, 1987. doi:10.1016/0002-9149(87)91189-1.
49. **Kitabatake A**, **Inoue M**, **Asao M**, **Masuyama T**, **Tanouchi J**, **Morita T**, **Mishima M**, **Uematsu M**, **Shimazu T**, **Hori M**, **Abe H.** Noninvasive evaluation of pulmonary hypertension by a pulsed Doppler technique. *Circulation* 68: 302–309, 1983. doi:10.1161/01.CIR.68.2.302.
50. **Martin-Duran R**, **Larman M**, **Trugeda A**, **De Prada JA**, **Ruano J**, **Torres A**, **Figueroa A**, **Pajaron A**, **Nistal F.** Comparison of Doppler-determined elevated pulmonary arterial pressure with pressure measured at cardiac catheterization. *Am J Cardiol* 57: 859–863, 1986. doi:10.1016/0002-9149(86)90627-2.
51. **Blackburn MR**, **Lee CG**, **Young HW**, **Zhu Z**, **Chunn JL**, **Kang MJ**, **Banerjee SK**, **Elias JA.** Adenosine mediates IL-13–induced inflammation and remodeling in the lung and interacts in an IL-13–adenosine amplification pathway. *J Clin Invest* 112: 332–344, 2003. doi:10.1172/JCI16815.
52. **Rath M**, **Müller I**, **Kropf P**, **Closs EI**, **Munder M.** Metabolism via arginase or nitric oxide synthase: two competing arginine pathways in macrophages. *Front Immunol* 5: 532, 2014. doi:10.3389/fimmu.2014.00532.
53. **Asosingh K**, **Lauruschkat CD**, **Alemagno M**, **Frimel M**, **Wanner N**, **Weiss K**, **Kessler S**, **Meyers DA**, **Bennett C**, **Xu W**, **Erzurum S.** Arginine metabolic control of airway inflammation. *JCI Insight* 5: e127801, 2020. doi:10.1172/jci.insight.127801.
54. **Tabeling C**, **Wienhold SM**, **Birnhuber A**, **Brack MC**, **Nouailles G**, **Kershaw O**, **Firsching TC**, **Gruber AD**, **Lienau J**, **Marsh LM**, **Olschewski A**, **Kwapiszewska G**, **Witzenrath M.** Pulmonary fibrosis in Fra-2 transgenic mice is associated with decreased numbers of alveolar macrophages and increased susceptibility to pneumococcal pneumonia. *Am J Physiol Lung Cell Mol Physiol* 320: L916–L925, 2021. doi:10.1152/ajplung.00505.2020.
55. **Steffes LC**, **Froistad AA**, **Andruska A**, **Boehm M**, **McGlynn M**, **Zhang F**, **Zhang W**, **Hou D**, **Tian X**, **Miquerol L**, **Nadeau K**, **Metzger RJ**, **Spiekerkoetter E**, **Kumar ME.** A Notch3-marked subpopulation of vascular smooth muscle cells is the cell of origin for occlusive pulmonary vascular lesions. *Circulation* 142: 1545–1561, 2020. doi:10.1161/CIRCULATIONAHA.120.045750.
56. **Jais X**, **Launay D**, **Yaici A**, **Le Pavec J**, **Tchérakian C**, **Sitbon O**, **Simonneau G**, **Humbert M.** Immunosuppressive therapy in lupus- and mixed connective tissue disease–associated pulmonary arterial hypertension: a retrospective analysis of twenty-three cases. *Arthritis Rheum* 58: 521–531, 2008. doi:10.1002/art.23303.
57. **Tabeling C**, **Yu H**, **Wang L**, **Ranke H**, **Goldenberg NM**, **Zabini D**, **Noe E**, **Krauszman A**, **Gutbier B**, **Yin J**, **Schaefer M**, **Arenz C**, **Hocke AC**, **Suttorp N**, **Proia RL**, **Witzenrath M**, **Kuebler WM.** CFTR and sphingolipids mediate hypoxic pulmonary vasoconstriction. *Proc Natl Acad Sci USA* 112: 25829545, 2015. doi:10.1073/pnas.1421190112.
58. **Wang L**, **Yin J**, **Nickles HT**, **Ranke H**, **Tabuchi A**, **Hoffmann J**, **Tabeling C**, **Barbosa-Sicard E**, **Chanson M**, **Kwak BR**, **Shin HS**, **Wu S**, **Isakson BE**, **Witzenrath M**, **de Wit C**, **Fleming I**, **Kuppe H**, **Kuebler WM.** Hypoxic pulmonary vasoconstriction requires connexin 40–mediated endothelial signal conduction. *J Clin Invest* 122: 4218–4230, 2012. doi:10.1172/JCI59176.
59. **Ward JP**, **McMurtry IF.** Mechanisms of hypoxic pulmonary vasoconstriction and their roles in pulmonary hypertension: new findings for an old problem. *Curr Opin Pharmacol* 9: 287–296, 2009. doi:10.1016/j.coph.2009.02.006.
60. **Spin JM**, **Nallamshetty S**, **Tabibiazar R**, **Ashley EA**, **King JY**, **Chen M**, **Tsao PS**, **Quertermous T.** Transcriptional profiling of in vitro smooth muscle cell differentiation identifies specific patterns of gene and pathway activation. *Physiol Genomics* 19: 292–302, 2004. doi:10.1152/physiolgenomics.00148.2004.
61. **Tsujino K**, **Li JT**, **Tsukui T**, **Ren X**, **Bakiri L**, **Wagner E**, **Sheppard D.** Fra-2 negatively regulates postnatal alveolar septation by modulating myofibroblast function. *Am J Physiol Lung Cell Mol Physiol* 313: L878–L888, 2017. doi:10.1152/ajplung.00062.2017.
62. **Fagan KA**, **Fouty BW**, **Tyler RC**, **Morris KG**, **Hepler LK**, **Sato K**, **LeCras TD**, **Abman SH**, **Weinberger HD**, **Huang PL**, **McMurtry IF**, **Rodman DM.** The pulmonary circulation of homozygous or heterozygous eNOS-null mice is hyperresponsive to mild hypoxia. *J Clin Invest* 103: 291–299, 1999. doi:10.1172/JCI3862.
63. **Yang Z**, **Ming XF.** Arginase: the emerging therapeutic target for vascular oxidative stress and inflammation. *Front Immunol* 4: 149, 2013. doi:10.3389/fimmu.2013.00149.
64. **Durante W**, **Johnson FK**, **Johnson RA.** Arginase: a critical regulator of nitric oxide synthesis and vascular function. *Clin Exp Pharmacol Physiol* 34: 906–911, 2007. doi:10.1111/j.1440-1681.2007.04638.x.
65. **Farmakis IT**, **Demerouti E**, **Karyofyllis P**, **Karatasakis G**, **Stratinaki M**, **Tsiapras D**, **Athanassopoulos G**, **Voudris V**, **Giannakoulas G.** Echocardiography in pulmonary arterial hypertension: is it time to reconsider its prognostic utility? *J Clin Med* 10: 2826, 2021. doi:10.3390/jcm10132826.
66. **Blalock S**, **Chan F**, **Rosenthal D**, **Ogawa M**, **Maxey D**, **Feinstein J.** Magnetic resonance imaging of the right ventricle in pediatric pulmonary arterial hypertension. *Pulm circ* 3: 350–355, 2013. doi:10.4103/2045-8932.114763.